2008

Automotive Battery State-of-Health Monitoring Methods

Ryan J. Grube
Wright State University

AUTOMOTIVE BATTERY STATE-OF-HEALTH MONITORING METHODS

A thesis submitted in partial fulfillment
of the requirements for the degree of
Master of Science in Engineering

By

RYAN J. GRUBE
B.A., Kent State University, 1998

2008
Wright State University

WRIGHT STATE UNIVERSITY

SCHOOL OF GRADUATE STUDIES

December 17, 2008

I HEREBY RECOMMEND THAT THE THESIS PREPARED UNDER MY SUPERVISION BY Ryan J. Grube ENTITLED Automotive Battery State-of-Health Monitoring Methods BE ACCEPTED IN PARTIAL FULFILLMENT OF THE REQUIREMENTS FOR THE DEGREE OF Master of Science in Engineering.

_____
Xiaodong Zhang, Ph.D.
Thesis Director

_____
Kefu Xue, Ph.D.
Department Chair

Committee on
Final Examination

_____
Xiaodong Zhang, Ph.D.

_____
Kuldip Rattan, Ph.D.

_____
Hong Huang, Ph.D.

_____
Joseph F. Thomas, Jr., Ph.D.
Dean, School of Graduate Studies

ABSTRACT

Grube, Ryan James. M.S.E., Department of Electrical Engineering, Wright State University, 2008, Automotive Battery State-of-Health Monitoring Methods.

Effective vehicular power management requires accurate knowledge of battery state, including state-of-charge (SOC) and state-of-health (SOH). An essential functionality of automotive batteries is delivering high power in short periods to crank the engine. A well-known approach to battery SOH monitoring is to infer battery state-of-health from battery impedance or resistance, which is not robust to variation of battery types. The research and development of more reliable battery state-of-health monitoring methods to ensure vehicle start-up ability are presented in this thesis. The methods include a battery cranking voltage based method, a parity-relation based method using battery voltage and cranking current signals, and a support vector machine based pattern recognition method utilizing battery voltage and engine cranking speed. The performances of these methods have been evaluated and compared through analysis of extensive real vehicle cranking data from 2 vehicles and 20 batteries. Cost benefit analysis is also conducted with different sensor options.

CONTENTS

LIST OF FIGURES

LIST OF TABLES

ACKNOWLEDGEMENTS

I would like to express my gratitude to my advisor, Dr. Xiaodong Zhang, for giving me the opportunity to gain research experience alongside of him. His guidance and patience are most appreciated. I would also like to thank the General Motors Research and Development Center for funding this research and the technical help from Dr. Kwang-Keun Shin and Dr. Mutasim Salman. Also, I would like to thank Dr. Rattan and Dr. Huang for their comments to improve this thesis. Finally, I would like to thank my wife and children for their love, support, and sacrifices made through this endeavor.

CHAPTER 1
INTRODUCTION

The number of electrical devices in modern vehicles has been rapidly increasing in the last two decades, and this trend will accelerate [1][2][3]. The vehicle electric power system is required to supply sufficient power not only to safety related systems such as rear window defogger, anti-lock braking, and stability enhancement system, but also to comfort, convenience and entertainment features such as air conditioning, seat heating, audio, and video systems. The advent of new technologies such as X-by-wire is putting additional demand on the battery. The electric power management system serves to balance the power demanded and supplied as well as to ensure the vehicle's start-up ability. To achieve these goals, accurate and reliable knowledge of the battery state is essential [4][5][6].

On-board state-of-health (SOH) information is usually derived from parameters of an equivalent circuit battery model [5][6][7][8]. Many model-based methods require the use of a costly current sensor to measure high current (e.g., up to 1000 amps) during engine cranking. Additionally, those methods use constant thresholds (or limit values) on selected battery model parameters to determine battery end-of-life. However, the calibration of such constant thresholds is a difficult task due to the variations of battery types, vehicle starting systems, and operating environments.

A well-known approach to battery fault diagnosis/prognosis is to infer battery SOH from battery impedance or resistance (see, for instance, [6][7][8][9]). Battery SOH information from resistance measurements is valuable. However, to provide more accurate and robust battery diagnosis/prognosis, the battery resistance needs to be combined with other features via an integrated algorithm [7][8].

The following sections in Chapter 1 provide background information concerning the physical and chemical structure of the automotive lead-acid battery, the chemical reactions occurring within the battery, the engine cranking process, battery state-of-health monitoring, and an outline of the remainder of this thesis.

1.1 Automotive Lead-Acid Battery

A battery is an electrochemical device that stores electrical energy in a chemical form [10]. A chemical reaction occurs, between the active materials within the battery, to produce current whenever there is a load demand. An automotive battery is required to perform several functions:

- It supplies power to crank the engine. The cold cranking amperage required to start an internal combustion engine can be in excess of 800A.
- With the engine running, it supplies power to safety and luxury related features when alternator output isn't sufficient.
- It stabilizes the voltage for the electrical system. The battery provides protection from excessively high voltages that would otherwise damage other components in the electrical system.

- It keeps the vehicle running in the event of an alternator failure. Typical car batteries have a reserve capacity of 50-100 minutes [10].
- While the engine is off, it supplies power to accessories (e.g., power door locks, power seats, and anti-theft system).

Thus, the automotive battery plays an important role in ensuring successful engine starting and operation of high reliability safety features and comfort features employed within the vehicle.

1.1.1 Physical and Chemical Structure

The basic structure of an automotive lead-acid battery consists of a polypropylene case partitioned into six cell compartments with one cell element located within each compartment. These cell elements are submerged in an electrolyte and connected in series from the positive terminal post to the negative terminal post.

Within each of the six cell compartments are cell elements consisting of plates of dissimilar material, separators, and connecting links. Plates are formed by pasting soft material onto flat and sturdy, mesh-like grids constructed of a lead-calcium alloy [10]. Grids pasted with lead dioxide (PbO_2) form the positive plates (i.e., positive electrodes), while grids pasted with sponge lead (Pb) form the negative plates (i.e., negative electrodes). Groups of positive plates are alternately interlaced with groups of negative plates forming a cell element. Each plate of opposite polarity is separated with a porous envelope separator to allow electrolyte through and prevent plates from contacting each other and producing a short-circuit [10]. The six cell elements are connected in series using inter-cell links to connect the negative plates of one cell element to the positive

plates of the adjacent cell element. The positive plates and negative plates at opposite ends of the battery are connected to the positive and negative terminal posts, respectively. Each cell element can provide approximately two volts. Hence, a six cell automotive battery can provide 12V.

Each cell element contained within one of the six compartments is submerged in an electrolyte. A fully charged battery has an electrolyte composition consisting of approximately 36% sulfuric acid (H_2SO_4) and 64% pure water (H_2O). The specific gravity of this electrolytic solution is 1.270. This means that the electrolytic solution weighs 1.270 times that of pure water. The more dilute the electrolyte (i.e., higher water concentration) the lower the specific gravity (i.e., more like water). As the battery is discharged, the electrolyte becomes more concentrated with water molecules, lowering the specific gravity of the electrolyte. During charging, the specific gravity of the electrolyte increases causing the electrolyte to return to similar concentrations of sulfuric acid and water that were present in the original composition. This observation and measure of the specific gravity of the electrolyte can be used to determine the state-of-charge (SOC) of the battery which will be discussed in a later section.

1.1.2 Chemical Reactions

The chemical reaction between the dissimilar materials of the plates and the electrolyte produce a flow of electrons. During battery discharging, a chemical reaction occurs between the electrolyte and each negative and positive plate causing the release and absorption of electrons, respectively. In general, the total discharge reaction of the lead-acid battery is given in (1).

$$Pb + PbO_2 + 2 \cdot H_2SO_4 \Rightarrow 2 \cdot PbSO_4 + 2 \cdot H_2O \quad (1)$$

The sulfuric acid in the electrolyte dissociates into hydrogen and sulphite ions (SO_4). The lead (Pb) from the negative plates reacts with the sulphite ions (SO_4) forming lead sulphate $(PbSO_4)$. The lead and oxygen from the lead dioxide (PbO_2) pasted positive plates dissociates, releasing oxygen into the electrolyte which combines with the hydrogen ions in the electrolyte to form a rising concentration of water (H_2O). The oxygen-free lead ions (Pb) from the positive plates react with the sulphite ions (SO_4) in the electrolyte forming lead sulphate $(PbSO_4)$. Thus, lead sulphate $(PbSO_4)$ is produced on both the negative and positive plates and the electrolyte becomes more highly concentrated with water, lowering the specific gravity. Dilution of the electrolyte with water (H_2O) and accumulation of lead sulphate $(PbSO_4)$ on the plates stops the chemical reaction, therefore completing the discharge [10][11].

More specifically, for the conversion into electrical energy during discharging, the total chemical reaction has to be separated into two plate reactions, one that releases electrons (i.e., at the negative plate), and one that absorbs electrons (i.e., at the positive plate) [11]. At the negative plates, lead (Pb) is oxidized to (Pb^{2+}) ions releasing two electrons, and at the positive plates, (Pb^{4+}) ions are reduced to (Pb^{2+}) ions absorbing two electrons [11] given in (2).

$$Pb \Rightarrow Pb^{2+} + 2 \cdot e^- \quad \text{and} \quad Pb^{4+} + 2 \cdot e^- \Rightarrow Pb^{2+} \quad (2)$$

Within the electrolyte of automotive lead-acid batteries, dilute sulfuric acid (H_2SO_4) mainly dissociates into $(2 \cdot H^+)$ and (SO_4^{2-}) during discharge [11]. Therefore, the reaction at the negative plate is given by (3). Lead (Pb) is oxidized to divalent lead ions (Pb^{2+}), and lead sulphate $(PbSO_4)$ forms, releasing two electrons.

$$Pb + H^+ + HSO_4^- \Rightarrow PbSO_4 + 2 \cdot H^+ + 2 \cdot e^- . \quad (3)$$

The reaction at the positive plate is given in (4). Lead ions (Pb^{4+}) are reduced to the divalent lead ions (Pb^{2+}) and lead dioxide (PbO_2) is converted into lead sulfate $(PbSO_4)$ resulting in the absorption of two electrons.

$$PbO_2 + HSO_4^- + 3 \cdot H^+ + 2 \cdot e^- \Rightarrow PbSO_4 + 2 \cdot H_2O . \quad (4)$$

Combining (3) and (4), the sum of both negative and positive plate reactions is the cell reaction given in (5). This results in a flow of electrons from the negative plates to the positive plates during discharging.

$$Pb + PbO_2 + 2 \cdot H^+ + 2 \cdot HSO_4^- \Leftrightarrow 2 \cdot PbSO_4 + 2 \cdot H_2O \quad (5)$$

During charging of the lead-acid battery, the chemical reaction in (5) is reversed. Lead sulphate $(PbSO_4)$ on both plates dissociates into lead ions and sulphite ions (SO_4), and water in the electrolyte dissociates into hydrogen and oxygen. The sulphite ions

(SO_4) recombine with hydrogen from the electrolyte producing sulfuric acid (H_2SO_4), raising the specific gravity of the electrolyte. The negative plates return to their original lead (Pb) form [10], and the lead ions (Pb) at the positive plates recombine with oxygen from the electrolyte forming the original lead dioxide composition (PbO_2). This total reaction causes a flow of electrons from the positive plates back to the negative plates.

1.1.3 Battery State

Effective vehicular power management requires accurate and reliable knowledge of the battery state. The battery state is represented by state-of-charge (SOC) and state-of-health (SOH). Battery performance is dependent upon the state-of-charge and state-of-health of the battery. In order to be able to detect limited battery functionality, it is essential to measure or estimate these properties [4].

The battery SOC represents the stored power and energy available. State-of-charge (SOC) is the percentage of the actual amount of charge compared with the full charge [12].

$$\mathrm{SOC} = \frac{\text{actual amount of charge}}{\text{amount of total charge}} * 100\% \tag{6}$$

One method to estimate battery SOC externally is to measure the equilibrium open circuit voltage (OCV) after the battery has relaxed for an extended period of time. Because the specific gravity of the electrolyte, the open circuit voltage (OCV), and the SOC of a battery have a nearly linear relationship, the state-of-charge can be determined from a look-up table [8][10].

Another existing method to estimate battery SOC uses the coulomb counting method. This method is based on current integration. The change in battery state-of-charge (ΔSOC) due to charging or discharging is given by (7), where $\eta_{(I)}$ is the charging efficiency, β_T is the temperature coefficient with rated capacity, and Cap_{rated} is the rated capacity of the battery [13][14].

$$\Delta SOC = \frac{\int_{t_0}^{t} \eta_{(I)} I_{bat} dt}{[\beta_T] Cap_{rated}} \tag{7}$$

The battery's net cumulative charge is determined then as the difference between the previous SOC and ΔSOC as, $SOC_{net} = SOC_0 - \Delta SOC$. Throughout this research, this method is used to estimate the SOC of batteries used during vehicle test cranking.

Battery SOH is an indication of power capability and battery capacity and depends on battery SOC and temperature. Poor battery performance can be caused by low SOH and/or low SOC. Thus, an automotive battery may be unable to meet one demand (e.g., cranking), but is ready to meet other vehicle electric demands (e.g., lighting and power locks) [12] or vice versa. Therefore, battery SOH includes cranking power SOH, which is a measure of the battery's ability to start the vehicle, and capacity SOH, which is a measure of the battery's ability to meet reserve capacity requirements.

1.1.4 Battery Aging and Service Life

Material changes and transport of substances are the most basic processes within a battery. In large part, stresses to the battery material age the battery and determine its service life. These stresses depend largely on the operating conditions of the battery (e.g., temperature and number of discharge/charge cycles). Many parameters influence battery aging and battery service life. Temperature, being one of these parameters, has a decisive influence on battery aging and service life. Increased temperature speeds up the rate of most electrochemical reactions whether they are desirable or undesirable.

Undesirable electrochemical reactions are called aging factors in batteries. Many of these aging factors are irreversible and ultimately cause battery failure. For lead-acid batteries, the predominant modes of failure are as follows:

- Grid corrosion in the positive plates. Due to the compact design of an automotive battery, grid corrosion may cause grid growth resulting in short-circuits between the positive plate and negative pole bridge [11]. Moreover, grid corrosion increases the internal resistance of the battery and reduces discharge voltage. Increased temperatures and overcharging at too-high a cell voltage contribute to grid corrosion.
- The disintegration of lead dioxide and re-crystallization of lead called sulfatation. This condition causes the negative electrode to lose capacity due to the formation of large lead sulfate crystals, thus reducing the active surface area. Sulfatation is aggravated by increased temperatures, repeated charge/discharge cycles, and plates that remain in a partly discharged state for prolonged periods [15].

- Positive active mass degradation and loss of coherence to the grid [15]. This condition is the result of the positive active material becoming so porous that contact between the positive active material and the grid is eventually lost. Prolonged cycling causes the active material to become softer and softer to the point of “shedding” or “sludging”.
- Water loss. Increases in water loss (aging of the electrolyte) contribute to shortened service life or battery failure. Electrolysis of water, as a result of overcharging, dissociates hydrogen from oxygen causing hydrogen gas evolution and ultimately water loss. Increased acid concentration increases the rate of self-discharge resulting in an insufficient SOC and sulfatation [15].
- Oxidation by oxygen intake. The intake of oxygen causes the negative plates to become partly discharged reducing the capacity of the negative plates and the battery state-of-charge [11].
- Short circuits. Short circuits can occur across the separators as a result of prolonged deep-discharge [15]. The concentration of sulfuric acid decreases significantly during deep-discharge. Large amounts of lead sulfate produced on the plates can fill the pores of the separators. During recharge, the lead sulfate in the pores of the separator may be converted into metallic lead deposits on the separators creating a short circuit between the positive and negative plate material.

1.2 Vehicle Engine Cranking

Successfully starting an internal-combustion engine requires that the engine is cranked at a speed (i.e., 50-100 rpm for cold starting) sufficient to make combustion possible and to give the flywheel sufficient momentum to keep rotating for a few firing strokes until the engine is capable of running unassisted [10]. In order for the engine to be cranked, a dc starter motor is required to produce high initial torque to rotate the ring gear of the flywheel to overcome the inertia of a stationary engine and transmission components [10].

A starter motor is a high torque dc motor that is designed to operate at extreme overload and high efficiency. Mounted on the starter motor is a solenoid consisting of a cylindrical plunger surrounded by a hold-in winding and a pull-in winding. The plunger operates a shift lever used to engage the pinion gear on the output shaft of the motor with the ring gear around the flywheel. The plunger also pushes a contact bar that closes the battery/motor circuit in order for high current to flow to energize the starter motor.

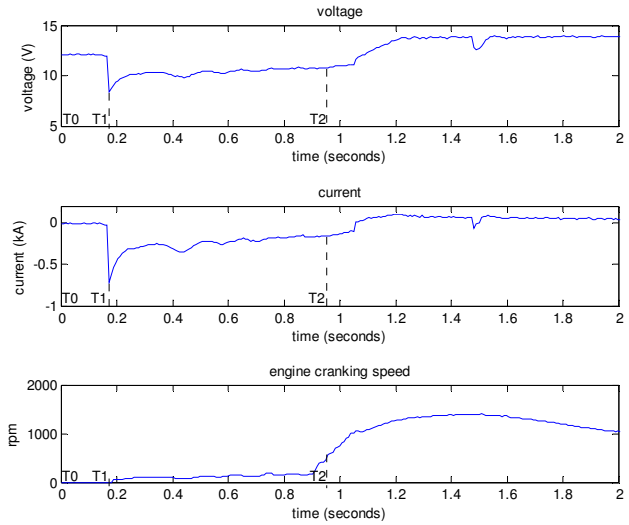

Figure 1: Battery voltage, current, and engine rpm waveforms during the engine cranking process.

Figure 1 shows typical voltage, current, and engine rpm waveforms for a successful engine start, where *T0* = 0, *T1* is the instant when the starter is engaged, and *T2* is the instant when engine cranking is successfully completed (i.e., about 500 rpm). The time from *T0* to *T2* defines the total engine start time. When the key is turned to the crank position at *T0*, the cranking procedure begins. The ignition switch closes, and an electrical delay follows from *T0* to *T1* where several pre-crank procedures occur such as fuel pressure initialization, a crank request received by the electronic control module (ECM), calibration delays, and the starter motor relay is commanded on. Once these pre-crank procedures are completed, current from the battery flows through the starter motor relay to the starter solenoid through a pull-in winding that electromagnetically pulls the plunger into the core causing the connected shift lever to push the pinion gear forward to mesh with the ring gear. Immediately after the mechanical connection between the pinion and ring gears is completed, the plunger pushes a contact bar at the rear of the solenoid. The contact bar closes the circuit between the battery and the motor allowing high current to flow from the battery to energize the motor. The events just described above are completed prior to time *T1*.

The time from *T1* to *T2* specifically defines the engine crank time. At time *T1*, the starter motor has just engaged, and its angular velocity is still zero. Since motor torque is directly proportional to the current supplied, maximum torque is produced when the armature (i.e., output shaft) is stationary (i.e., when angular velocity is zero) [10]. Hence, at time *T1*, the magnitude of $I(T1)$ is greatest at this instant of the cranking procedure and there is no back emf. A small proportion of this current flows through a hold-in winding keeping the plunger held in its active position.

Just after time *T1*, the starter motor begins rotating the flywheel through the pinion/ring gear mesh, thereby rotating the crankshaft. As can be seen in the engine cranking speed waveform plot of Figure 1, the crank shaft is being rotated at approximately 50-100 rpm for several tenths of a second prior to time *T2*. As the rotation speed of the starter motor increases, back emf increases proportionally opposing the current supply thereby reducing the current drawn from the battery to the starter motor [10]. This reduction in current is evident in the current waveform plot of Figure 1 where there is a sharp decrease in the magnitude of the current just after time *T1*. When the back emf has reached the level of the battery voltage, the starter motor will have reached its maximum speed.

The oscillations evident in the voltage and current waveforms after time *T1* in Figure 1 coincide with the compression and combustion strokes of the engine. During compression, more power (i.e., voltage and current) is needed to overcome the resistive forces of compression. Increased voltage and current magnitudes correspond to compression strokes whereas decreased voltage and current magnitudes correspond to the combustion strokes.

Finally, in the engine cranking speed waveform plot of Figure 1, after the engine cranking speed has reached approximately 500 rpm at time *T2*, the engine is capable of running without the assistance of the starter motor. At this time, the ignition switch is opened cutting current to the hold-in winding of the starter solenoid. A return spring forces the contact bar and plunger back to their resting positions de-energizing the starter motor and then disengaging the pinion/ring gear mesh to prevent overrunning the starter

motor. In Figure 1, the magnitudes of the voltage and current return to a steady state, approximately two-tenths of a second after time *T2*.

Engine cranking demands high power from the battery in a short period. This demand, as well as supplying power to other systems makes reliable battery operation imperative. Knowledge of the battery state, the battery's current condition, and future performance using battery state-of-health monitoring is essential to ensure that the battery is ready to perform high reliability functions on demand.

1.3 Battery State-of-Health Monitoring

1.3.1 Benefits of Battery State-of-Health Monitoring

It is the goal of this research to develop more robust and effective algorithms to monitor the automotive battery state-of-health (SOH). Knowledge of the battery SOH allows conclusions to be drawn about the battery's future performance, best use of its capability to supply power for high reliability devices, and more importantly its end-of-life and replacement. Accurate battery SOC and SOH information offered by battery monitoring will allow advanced power management strategies to be implemented; hence, achieving the following cost and safety related benefits:

- Reduction in fuel consumption and emission rates. First, accurate electric power management is essential to support advanced stop-start systems (i.e., micro hybrids), hybrid electric systems, and other engine efficiency solutions. Secondly, advanced power management can optimize the use of the alternator and

consequently fuel consumption by avoiding unnecessary charging of a battery at an adequate SOC.

- Extend battery life by maintaining an optimal battery SOC range. Consistently operating a lead-acid battery at low SOC will reduce the battery's service life.
- Improved vehicle safety by determining best use of the battery's capability for safety-related features. Monitoring of the battery state allows for advanced power management to either reduce electrical power consumption by selectively limiting operation of luxury functions or increase power generation by controlling the alternator, engine speed, or automatic gearbox control to guarantee sufficient power to operate safety-related features.
- Increased cranking reliability. Advanced power management can guarantee adequate future cranking power capability.
- Reduced incidences of vehicle breakdown due to low SOC and/or low SOH battery failures. The power management system can automatically charge the battery or provide replacement strategies to avoid ensuing vehicle breakdowns.
- Optimized battery and generator size and cost. Since the battery SOC can now be controlled accurately, larger batteries and alternators are no longer needed for marginal operating conditions.
- Reduced battery warranty cost. Accurate battery SOH information prevents mistaken replacement of batteries with a low SOC but good SOH.

1.3.2 Overview of Fault Diagnosis Methods

A fault is an undesirable deviation from normal behavior of a characteristic property of a variable. Approaches to fault diagnosis or detection are either model-based or qualitative (model-less). Model-based fault detection can be achieved using parameter estimation, state variable estimation and observers, and parity-relation equations. Below, the model-based fault diagnosis methods are briefly described.

- **Fault detection with parameter estimation.** Model parameters are constants or time-dependent coefficients that are part of a process model. The process model is a mathematical relationship between the input and output signals. For processes containing lumped parameters, dynamic process models are differential equations linearized about one operating point given by (8).

$$\begin{aligned} y(t) + a_1\dot{y}(t) + a_2\ddot{y}(t) + \ldots + a_n y^{(n)}(t) &= b_0 u(t) \\ + b_1\dot{u}(t) + b_2\ddot{u}(t) + \ldots + b_m u^{(m)}(t) & \end{aligned} \tag{8}$$

The model parameters $\theta^T = [a_1 \ldots a_n \vdots b_1 \ldots b_n]$ are the relationships of the coefficients of the physical process (e.g., mass, resistance, capacities). Faults occurring in the physical process constants will be expressed in the model parameters [16].

When changes in the physical process coefficients indicating faults cannot be measured directly, changes in the process model parameters, θ, can be used to detect faults. The following procedure describes the parameter estimation method [16]:

1) By theoretical modeling, establish the process equation, $Y(t) = f\{U(t), \theta\}$, for measurable input and output variables.
2) Determine relationships between model parameters θ_i and physical process coefficients p_j: $\theta = f(p)$.
3) Using the measurements of the signals $Y(t)$ and $U(t)$, estimate the model parameters θ_i.
4) Calculate the physical process coefficients, $p = f^{-1}(\theta)$, and determine their changes, Δp_j.
5) With a known relationship between process faults and changes in the physical process coefficients, possible process faults can be located.

This procedure combines theoretical modeling and parameter estimation of continuous-time models and require that $p = f^{-1}(\theta)$ exists [16].

- **Fault detection with state variable estimation and observers.** When internal, immeasurable process state variables indicate process faults, these state variables can be estimated from measurable signals with the use of a known process model. In general, dynamic relationships, $X(t) = f\{U, Y, t\}$, exist within the automotive battery. To linearize these dynamic relationships about one operating point, the state representation is given by (9) and (10), where $y = \Delta Y$, $u = \Delta U$, $x = \Delta x$ are the changes of *Y*, *U*, and *X*, respectively [16].

$$\dot{x}(t) = Ax(t) + Bu(t) \tag{9}$$

$$y(t) = Cx(t) \tag{10}$$

Assuming that A, B, and C are known process parameters, using a state variable observer (deterministic case) or state variable filter (stochastic case) with a properly designed feedback matrix H, the immeasurable state variables can be estimated from the input and output signals [16][17], where $e(t)$ is the output error given in (11) and (12).

$$\hat{\dot{x}}(t) = A\hat{x}(t) + Bu(t) + He(t) \tag{11}$$

$$e(t) = y(t) - C\hat{x}(t) \tag{12}$$

With a stable observer, changes in the process (i.e., noise and faults) can be modeled by $v(t)$ and sensor faults by $\mu(t)$ in (13) and (14), respectively, where $\upsilon(t)$ is process faults and $n(t)$ is noise from measurement.

$$\dot{x}(t) = Ax(t) + Bu(t) + F\upsilon(t) + v(t) \tag{13}$$

$$y(t) = Cx(t) + n(t) + \mu(t) \tag{14}$$

Abrupt changes of the states and the outputs can be detected using Kalman-Bucy filters where residuals are generated [16]. Faults can then be detected by comparing the residual with a designed threshold.

- **Fault detection with parity-relation techniques.** This model-based method, requiring known process model parameters, runs a fixed model G_M parallel to the process G_P to produce an output error given in (15).

$$r'(s) = [G_P(s) - G_M(s)]u(s) \tag{15}$$

Residuals are generated by (16) for additive input and output faults if $G_P(s) = G_M(s)$. The input and output signal faults are f_u and f_y, respectively. The generated residuals can then be compared to a designed threshold to pinpoint faults [17].

$$r'(s) = G_P(s) f_u(s) + f_y(s) \tag{16}$$

Some qualitative (model-less) approaches to fault diagnosis have also been considered, such as pattern recognition methods, inference methods (e.g., expert systems, fuzzy systems) and a combination of these two approaches [18][19][20]. An obvious advantage of these approaches is that a good mathematical model of the monitored system is not required. However, qualitative methods are relatively ambiguous and crude, which usually result in more missed faults and false alarms.

1.3.3 Previous Work

The ever increasing number of auxiliary features installed in today's cars requires careful monitoring and control of the energy balance to avoid electrical system weakness [11]. The automotive battery is required to assist in many high reliability functions such as engine cranking, anti-lock braking, and lighting. Just as knowing the amount of remaining fuel in the vehicle's gas tank is important for future operation, knowledge of the battery's amount of charge, capacity, and overall health are essential for successful future operation of the vehicle. Many methods have been proposed to monitor the current state of the automotive battery and predict the overall health and future performance of the battery. The most common approaches to monitor battery SOH are based on resistance estimation and analysis of the parameters from a highly sophisticated battery model [5][6][7][8].

It has been well documented that battery internal resistance increases with the age of the battery. Many methods available are based on continually measuring parameters such as the voltage, charging or discharging current, and temperature of the battery in order to derive the internal resistance or impedance of the battery. The battery terminal voltage is measured at different discharge currents to estimate the internal resistance of the battery which is comprised of the ohmic resistance within the electrodes and electrolyte [11]. Using Ohm's Law, the resistance is calculated as the quotient of the change in voltage and the change in current. By analyzing the internal resistance/impedance data, thresholds are set to determine the battery's end-of-life. The problems with these methods are two fold. First, they are not robust to variation of battery types. All batteries are not manufactured equally, and there is no control over

which battery the driver may install in the vehicle. Since different batteries demonstrate higher internal resistance than others, constant adjustment to parameter thresholds is required. Secondly, costly high current sensors are required in order to derive internal resistance measurements of the battery.

State-of-health monitoring methods based on analyzing parameters of an equivalent circuit battery model are also common practice [5][6][7][8]. Many of these methods require use of a current sensor and use of constant thresholds on selected battery model parameters. A model-based method used in recent years is a galvanostatic non-destructive technique to monitor the battery state-of-health by analyzing impedance parameters [21]. This proposed method discharges the battery galvanostatically at a low rate over a short duration in order to obtain the ohmic resistance, charge-transfer resistance, and interfacial capacitance. In another method, the authors of [22] analyzed data obtained from impedance measurements over a wide range of frequencies and coulomb counting techniques. Fuzzy logic mathematics was then applied to determine battery SOC and SOH [22]. Linear or nonlinear observers, based on the Kalman Filter, Extended Kalman Filter and a generic cell model, have been employed to predict the state-of-charge and state-of-health of lead-acid batteries in [23].

1.4 Outline

An essential functionality of automotive batteries is to deliver high power in short periods, for instance, to crank the engine. This paper presents more reliable state-of-health monitoring algorithms for automotive lead-acid batteries to ensure a vehicle's start-up ability. Specifically, this thesis has four main contributions. First, a new battery

model during engine cranking is developed. Based on extensive analysis of various vehicle cranking data, battery ohmic behavior and voltage loss have been clearly observed. The proposed new battery model, which takes into account both the battery's voltage loss and ohmic behavior, is more accurate and computationally efficient than conventional methods.

Second, a battery cranking voltage based SOH monitoring method was developed by employing characteristics of the battery voltage signal during vehicle starting. This method doesn't require a costly high cranking current sensor. Moreover, battery end-of-life is determined based on particular features of the battery voltage signal during vehicle starting, so that algorithm calibration is much easier [24].

Third, a parity-relation based SOH monitoring algorithm was developed by using battery cranking voltage and current signals. Analysis of various cranking data has indicated that, in addition to battery resistance, battery voltage loss during cranking also provides valuable information of battery SOH. A calibrated parity-relation, characterizing the dynamics of good batteries during vehicle cranking, is used to estimate battery cranking voltage given a current signal. A residual, generated as the discrepancy between the actual voltage measurement and its estimation, is used to infer battery SOH. Through analysis of the residual based on a battery model during cranking, it is shown that the residual integrates the SOH information provided by both battery resistance and voltage loss, hence enhancing fault sensitivity and diagnostic/prognostic robustness [25].

Finally, it has been observed in this research that a correlation between battery SOH and engine cranking speed exists. On-line model-based fault diagnosis using engine cranking speed is difficult due to the complicated engine dynamics involved in

modeling the engine cranking process. Therefore, a support vector machine based pattern recognition method was developed utilizing features of battery voltage and engine cranking speed during cranking. Rather than constructing a physics-based model, a statistical model was trained with data sets representing the battery voltage and engine cranking speed of fresh and aged batteries. Good separation between the fresh and aged classes of batteries enabled the support vector machine to effectively classify previously unseen test data and provide a percentage based estimation of battery SOH.

The remainder of this thesis is organized as follows. Chapter 2 describes the new battery model during engine cranking. Chapter 3 describes the motivation, analysis, and on-board implementation of the battery cranking voltage based SOH monitoring method. Examples of the battery cranking voltage based algorithm performance evaluation results are included. Chapter 2 and Chapter 3 are based on the conference paper titled, "Automotive Battery State-of-Health Monitoring: A Battery Cranking Voltage Approach" [24].

Chapter 4 describes the motivation, analysis, and on-board implementation of the parity-relation based SOH monitoring method. Examples of the parity-relation based algorithm performance evaluation results through analysis of extensive vehicle cranking data are included. This chapter is based on the conference paper titled "Automotive Battery State-of-Health Monitoring: A Parity-Relation Based Approach" [25].

Chapter 5 presents comparative studies to further evaluate the performance, cost, and benefits of the algorithms. Specifically, the conventional resistance based approach is compared to these two battery SOH monitoring methods; the battery cranking voltage based method and the parity-relation based method. The weakness of the conventional

resistance based method is shown with respect to variation of battery types. The robustness of the battery cranking voltage based approach and the parity-relation based approach in determining battery SOH for different types of batteries is also shown. Furthermore, the battery cranking voltage based approach is compared with the parity-relation based approach to analyze the benefit with the use of an additional cranking current sensor.

Chapter 6 provides a brief introduction to support vector machines and the motivation and analysis of the support vector machine based pattern recognition method for battery SOH monitoring. Examples of the performance evaluation results through analysis of vehicle cranking data collected weekly from 10 Johnson Control LN3 batteries are also included. Finally, Chapter 7 discusses the conclusions from this research and future research including capacity-based SOH monitoring methods and methods capable of predicting the remaining useful life of a battery.

CHAPTER 2

BATTERY MODEL DURING ENGINE CRANKING

In this chapter, the battery dynamics during engine cranking are analyzed, and a new battery equivalent circuit model is presented. Compared with conventional battery models (e.g., [1][7][9]), the new model takes into account the battery's ohmic behavior and voltage loss during engine cranking. Therefore, it is a more accurate and computationally efficient representation of battery dynamics during engine cranking.

A widely used battery model for normal vehicle operations is the Thevenin battery model shown in Figure 2 (see, for example, [1][7][9][26][27]), where R_b is the ohmic resistance, V_{ocv} is the battery open circuit voltage, C_{dl} is the double layer capacitor, and R_{CT} is the charge transfer resistance. More sophisticated models have also been introduced, by including additional components such as a Warburg impedance [28], constant phase elements [28][29], or another RC component representing the diffusion process [30].

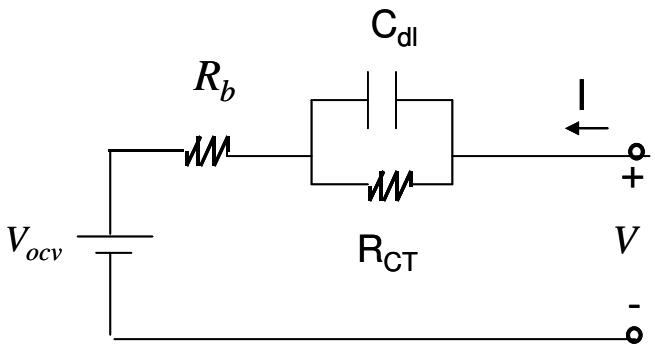

Figure 2: Thevenin battery model.

2.1 Battery Ohmic Behavior during Cranking

Typical battery current and voltage signals during vehicle cranking are given in Figure 3. To extract the portion of battery signals corresponding to the short period of vehicle cranking, the following procedure is applied. First, the voltage and current data samples corresponding to initial cranking voltage drop are located. Second, starting from that position, we locate the next sample whose battery current is greater than -100 A, which indicates the end of the cranking process. The data between these two samples characterizes the battery current and voltage signals during cranking. The extracted voltage and current data is plotted in Figure 4.

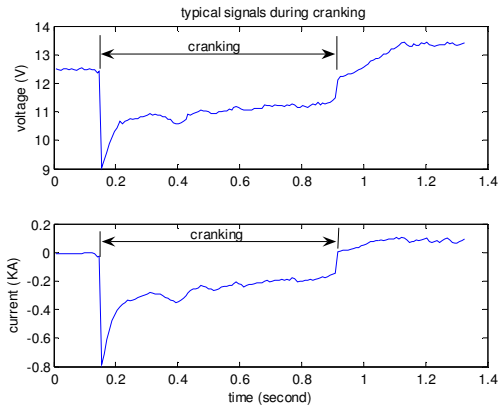

Figure 3: Typical signals of battery voltage and current during engine cranking.

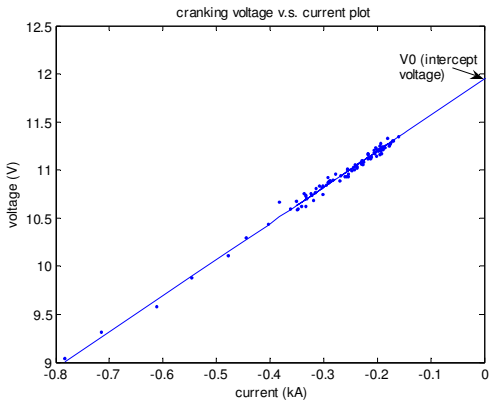

Figure 4: Extracted signal in a V-I plot (the linear least squares fit line is also shown).

The ohmic relationship between battery voltage and current can be clearly seen, which justifies the simplified model during vehicle cranking shown in Figure 5. In other words, the extra double layer RC components given in Figure 2 or other more complicated components, [27][28][29][30], are not needed to model the battery dynamics during cranking. Therefore, the new model is more computationally efficient.

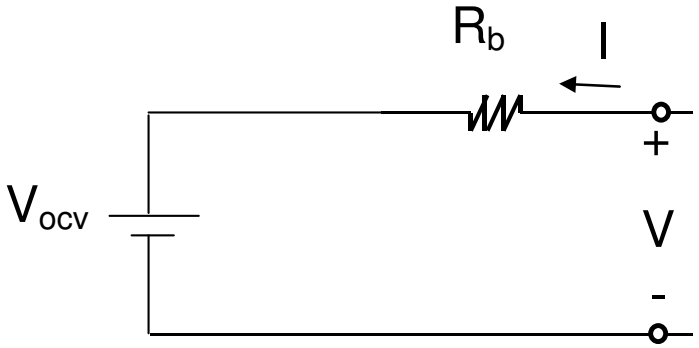

Figure 5: Voltage ohmic model.

2.2 Battery Voltage Loss during Cranking

In the battery ohmic model shown in Figure 5, the battery current and terminal voltage satisfies the following equation (17), where $I(t) < 0$ for discharge during cranking.

$$V(t) = V_{ocv} + I(t) * R_b \,. \tag{17}$$

In other words, the intercept voltage V_0 (i.e., the voltage corresponding to $I = 0$), shown in Figure 4, should be equivalent to the open circuit voltage V_{ocv}. However, extensive

analysis of various vehicle cranking data has indicated that the intercept voltage obtained from the V-I plot is lower than V_{ocv}, which is due to extra battery voltage loss during cranking.

The value of voltage loss can be estimated as

$$V_{loss} = V_{ocv} - V_o \ . \tag{18}$$

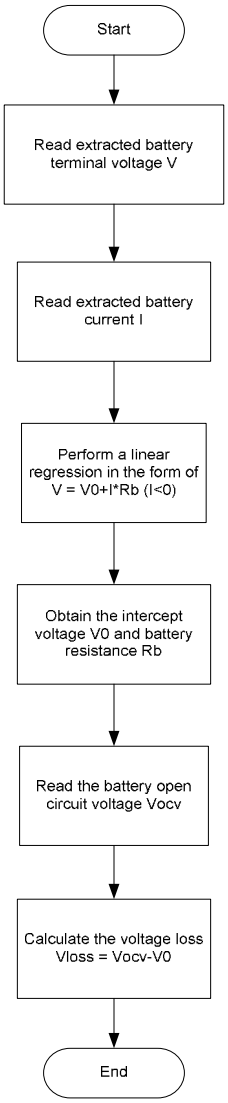

Figure 6: Flow chart for estimation of voltage loss.

A detailed procedure to compute V_{loss} is shown in Figure 6. We start with reading the extracted battery terminal voltage and current data, (i.e., V and I). Then, a least squares fit in the form of (19) is applied to estimate the intercept voltage V_0 and the battery resistance R_b.

$$V(t) = V_0 + I(t) * R_b \text{ , } (I(t) < 0 \text{ for discharge}), \tag{19}$$

More specifically, by defining $\theta = [V_0 \ R_b]^T$, $x = [1 \ I]^T$, and $\mathrm{y} = \mathrm{V}$, the above equation can be written in the form of equation (20).

$$y = x^T \theta . \tag{20}$$

By using linear least squares fit, an estimation of the unknown parameters are given by (21), where $X = \begin{bmatrix} 1 & I_1 \\ 1 & I_2 \\ \vdots & \vdots \\ 1 & I_n \end{bmatrix}$, $Y = \begin{bmatrix} V_1 \\ V_2 \\ \vdots \\ V_n \end{bmatrix}$, and n is the total number of samples collected during a cranking.

$$\theta = (X^T X)^{-1} X^T Y , \tag{21}$$

After V_0 is obtained, by using (17) and (19), the battery voltage loss is obtained from (18).

For instance, in Figure 4, the measured battery open circuit voltage before cranking is approximately 12.60 volts, while the intercept voltage computed from linear regression is approximately 11.95 volts. Therefore, the voltage loss is approximately 0.65 volts.

2.3 New Battery Model during Cranking

Based on the above analysis, a new battery model is developed, which takes into account both ohmic behavior and voltage loss during engine cranking. As illustrated in Figure 7, R_b is the battery internal resistance which represents the ohmic behavior of the battery, and V_{loss} is the battery voltage loss during cranking. By using V and I (I < 0 for discharge) to represent the battery terminal voltage and current, respectively, we have:

$$V(t) = V_{ocv} - V_{loss} + I(t) * R_b, (I(t) < 0) \tag{22}$$

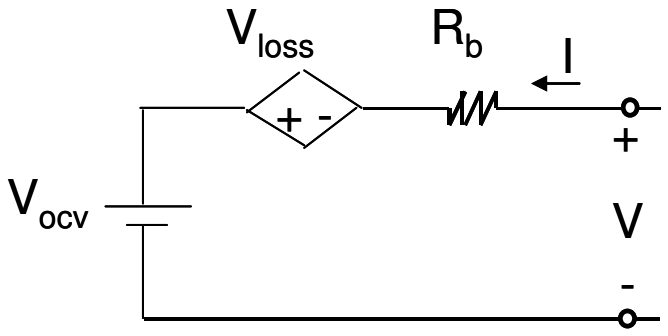

Figure 7: New battery model during cranking.

In general, V_{loss} can depend upon the current level. In this research, the focus is on high currents during cranking. Therefore, V_{loss} can be considered as a constant

throughout the cranking process. An example of the evaluation results of the new battery model is illustrated in Figure 8. The figure contains the plots of the actual battery voltage cranking data (solid line) and the battery cranking voltage based on the new battery model generated from (20). As can be seen in the figure, the battery cranking voltage generated from the new battery model closely approximates the actual battery voltage signal during cranking.

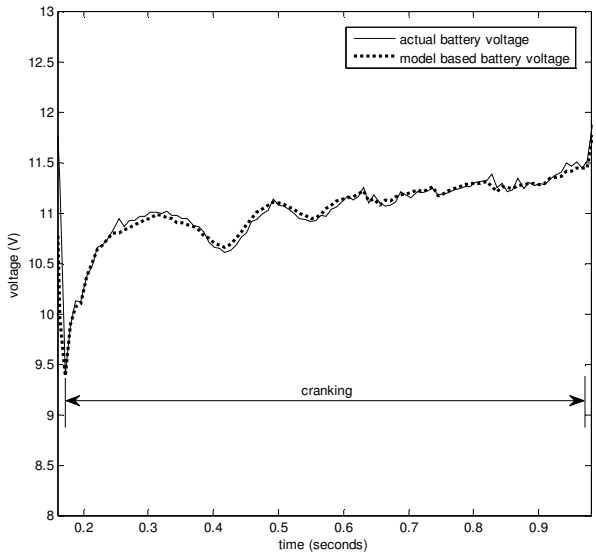

Figure 8: Comparison of new battery model based cranking voltage with actual cranking voltage signal.

CHAPTER 3

BATTERY CRANKING VOLTAGE BASED SOH MONITORING METHOD

An existing approach to determine battery SOH utilizes the minimum battery cranking voltage (i.e., at starter engagement). The minimum voltage based method uses a calibrated threshold on the minimum voltage during cranking to determine battery SOH. However, this approach is not very robust.

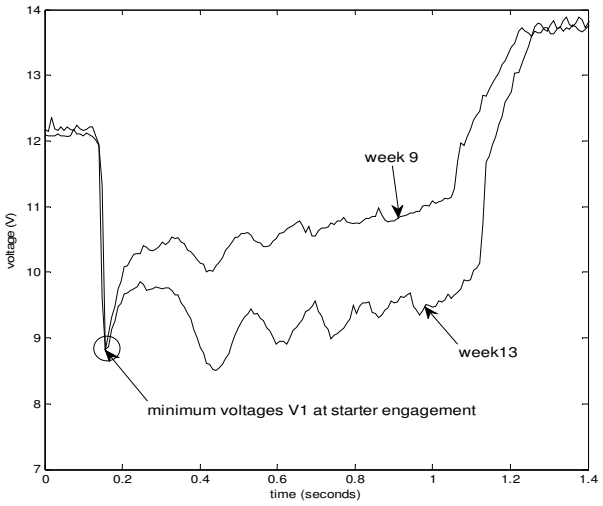

Figure 9: Battery cranking voltage signals.

Figure 9 shows the battery cranking voltage signals from a battery that was aged with accelerated aging procedures. This battery failed to crank the vehicle at week 14. The minimum voltage, *V1*, for week 9 (i.e., 5 weeks before cranking failure) and week 13

(i.e., 1 week before cranking failure) are approximately equal. The inherent problem with this approach is calibrating a threshold on *V1* that can discriminate between a battery that has some remaining useful life and a battery that is at end-of-life. In this example, setting a threshold at about 9 volts would surely cause a false alarm for the battery at week 9 that still has some remaining useful life. However, calibrating a threshold at about 8.5 volts to avoid misdiagnosis of the battery at week 9 would provide no pre-warning of pending cranking failure at week 14.

This chapter describes a battery cranking voltage based SOH monitoring method by using characteristics of the battery voltage signal during vehicle starting. This is an efficient method that doesn't require a costly high cranking current sensor compared to other methods such as the conventional resistance based approach. Moreover, algorithm calibration is much easier because battery end-of-life is determined based on particular features of the battery voltage signal during vehicle starting.

The basic idea of this SOH monitoring method consists of two steps. First, the cranking power capability of the battery is determined by comparing the battery voltage at the instant of starter engagement (i.e., *V1*) with the minimum voltage during the subsequent engine cranking phase. Second, with additional information of the battery SOC and temperature, battery SOH can be inferred. This method can be used to offer a pre-warning of battery end-of-life and avoid walk-home situations due to battery failures. Moreover, it can help to reduce battery no-trouble-found (NTF) and warranty cost.

In Section 3.1, we describe the characteristics of battery voltage during cranking for batteries with different power capabilities, which motivates the proposed battery SOH monitoring method. Based on the new battery model developed in Chapter 2, the battery

cranking voltage characteristics are analyzed in Section 3.2. Section 3.3 gives a detailed description of the proposed SOH monitoring algorithm. Section 3.4 includes examples of the battery cranking voltage based algorithm performance evaluation results through analysis of extensive vehicle cranking data collected from 10 field batteries and 10 Johnson Control LN3 batteries that were used in testing to crank two different vehicles.

3.1 Characteristics of Battery Voltage during Engine Cranking

In this research work, we have conducted extensive battery cranking tests using a variety of batteries collected from the field and production batteries aged through accelerated aging. A correlation between the battery cranking voltage characteristics and the cranking power capability has been consistently observed.

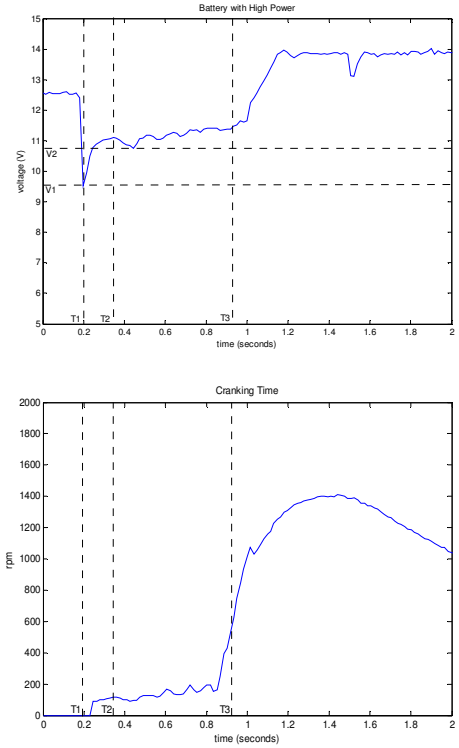

Figure 10: Battery voltage and engine rpm waveforms of a battery with high power.

Figure 10 shows a typical battery voltage signal (upper plot) and the corresponding engine RPM signal (lower plot) for a battery with sufficiently high starting power during vehicle starting. *T1* is the instant when the starter is engaged, *T2* is the instant when the battery voltage signal reaches its first peak after *T1*, *T3* is the instant when engine cranking is successfully completed, *V1* is the battery voltage at *T1*, and *V2* is the minimum battery voltage in the time interval [*T2, T3*]. As can be seen in Figure 10, if the battery power is high, we have *V2* > *V1*, that is, the minimum battery voltage during vehicle starting occurs at the instant of starter engagement (i.e., *T1)*, and the cranking process is successfully completed at a time less than 1 second.

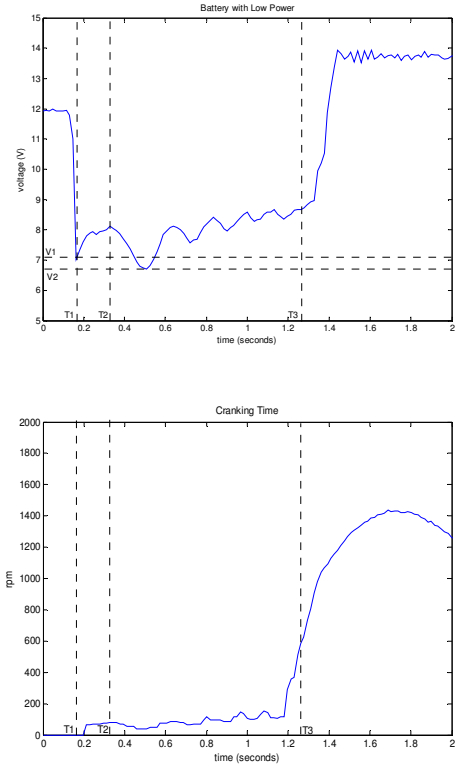

Figure 11: Battery voltage and engine rpm waveforms of a battery with low power.

In contrast, Figure 11 shows a typical battery voltage signal (upper plot) and the corresponding engine RPM signal (lower plot) for a battery with low starting power during vehicle starting. Comparing with Figure 10, it can be seen that the minimum battery voltage during vehicle starting does not occur at the instant of starter engagement, but during the subsequent engine cranking phase, (i.e., [*T2, T3*]). In other words, we have $V2 < V1$, which indicates that the battery's power is low. As can be seen, the cranking process is barely completed after 1.2 seconds. The battery needs to be replaced and/or recharged to avoid cranking failure.

The proposed battery cranking voltage based SOH monitoring method is motivated by the above observation of voltage characteristics during engine cranking. In order to develop an effective battery SOH monitoring algorithm, it is of great importance to understand the battery's dynamical behaviors during the engine cranking process presented in Chapter 2.

3.2 Analysis of Battery Cranking Voltage Characteristics

Figure 12 and Figure 13 show the typical cranking voltage and current waveforms of batteries with high power and low power, respectively. As shown in Figure 12, for a battery with high power, the voltage at *T1* (i.e., *V*(*T1*)) is less than the voltage at *T2* (i.e., *V*(*T2*)). However, for a battery with lower power, as shown in Figure 13, the voltage at *T1* is higher than the voltage at *T2*, (i.e., *V*(*T1*) > *V*(*T2*)).

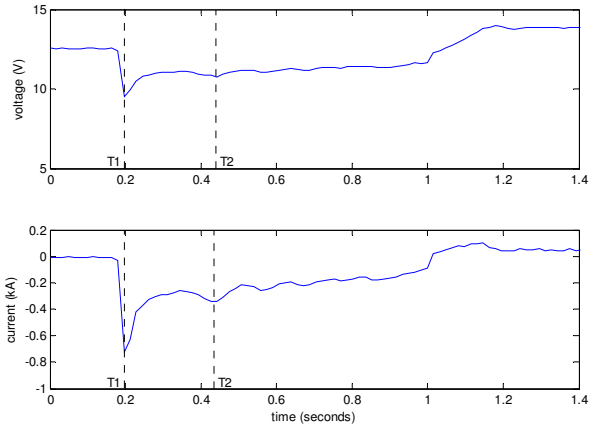

Figure 12: Typical voltage and current waveforms of a battery with high power.

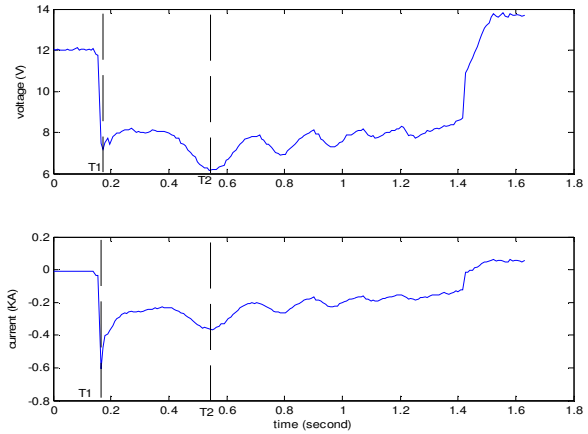

Figure 13: Typical voltage and current waveforms of a battery with low power.

Note that at *T1*, the starter motor is just engaged, and its angular velocity is still zero. Hence, there is no back emf at *T1*, and the magnitude of *I*(*T1*) is always largest throughout the cranking procedure regardless of the battery's power capability, (i.e., *I*(*T1*) < *I*(*T2*) for *I<0*), as can be seen from Figure 12 and Figure 13. Moreover, the open circuit voltage V_{ocv} should remain the same at *T1* and *T*2, since the battery SOC is unchanged. By using the battery model given in (22), we can see that, for a battery of low power, the fact that *V*(*T*2)<*V*(*T1*) implies that $V_{loss}(T2) > V_{loss}(T1)$ and/or

$R_b(T2) > R_b(T1)$. The increase of battery voltage loss and/or battery resistance indicates the battery's power capability is low, and battery dynamics are not stable during the cranking process. The battery should be replaced or recharged.

To get further insight into the cranking voltage based battery SOH monitoring method, the battery voltage and current signals corresponding to the cranking process in Figure 12 and Figure 13 are extracted and plotted in Figure 14 and Figure 15, respectively. As can be seen from Figure 14 (corresponding to Figure 12), if the battery has sufficiently high cranking power, the voltage difference, $\Delta V = V2 - V1 > 0$, and the cranking voltage and current has a good linear relationship. In contrast, Figure 15 (corresponding to Figure 13) shows that with a battery of low cranking power, the voltage difference, $\Delta V = V2 - V1 < 0$, and the relationship between cranking voltage and current becomes nonlinear. Extensive analysis of vehicle cranking data has shown that this type of strong nonlinear behavior is a good indication of low battery power or pending cranking failure.

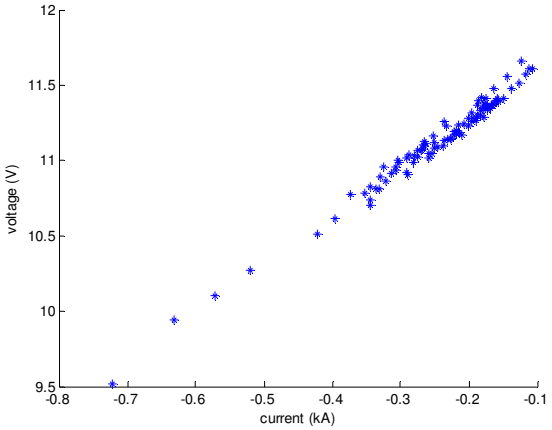

Figure 14: Extracted signals from Figure 12 in a V-I plot.

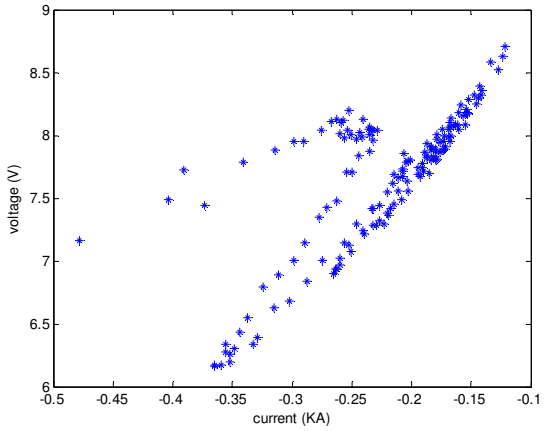

Figure 15: Extracted signal from Figure 13 in a V-I plot.

Note that while checking the relationship between voltage and current requires the use of an expensive high cranking current sensor, the battery cranking voltage based SOH monitoring method presented in this research is an indirect method without the need of a high current sensor. Moreover, the computation involved in on-board implementation is very simple.

3.3 Implementation of the Battery SOH Monitoring Algorithm

It is worth noting that a low voltage difference ΔV can be caused by low battery SOH and/or low SOC. To determine battery SOH, one approach is to define the threshold on ΔV as a function of SOC and temperature. An alternative method is to determine battery-end-of-life if ΔV is low (e.g., below zero) and battery SOC is above a certain calibrated level. To simplify the calibration process, in this research work the latter approach is adopted. Next, the proposed battery SOH monitoring algorithm using the battery's cranking voltage characteristics is described.

This SOH monitoring method consists of two steps. First, determine the cranking power capability of the battery by comparing the battery voltage at the instant of starter engagement with the minimum voltage during the subsequent engine cranking phase. Second, with additional information of the battery SOC and temperature, battery SOH can be inferred. More specifically, the inputs to the algorithm are the battery minimum voltage at the initial drop (*V1*), the battery minimum voltage after the first peak voltage during vehicle starting (*V2*), battery start-up SOC, and battery temperature. The specifications of the sensor signals and variables are listed in Table 1.

Table 1: Specifications of sensor signals and variables.

Battery signals	accuracy	resolution	range	# of samples	sampling rate
Voltage (V)	+/- 0.1	0.001	0 to 16	2	2 samples
Temperature (0C)	+/- 5	1	-40 to +80	1	1 sample
SOC (%)	+/- 10	1	0 to100	1	1 sample

The proposed on-board implementation of the algorithm has the following calibration parameters:

- A threshold *SOC_Threshold* calibrated as a 1x4 2-D look-up table as a function of *EBT* (estimated battery temperature) (e.g., 50°C, 25°C, 0°C, -18°C).
- A threshold ΔV*_Threshold* calibrated as a 1x4 2-D look-up table as a function of *EBT* (e.g., 50°C, 25°C, 0°C, -18°C).

It is worth noting that a positive constant for ΔV*_Threshold* is used instead of 0. The main objective is to offer a pre-warning before the battery's SOH is too low. Hence,

the driver can be informed in a timely manner before cranking failure to avoid walk-home situations. Moreover, the RVC (regulated voltage control) algorithm typically regulates battery SOC to 80%. By assuming 10% SOC estimation error and another 10% SOC loss due to parasitic load when the vehicle is off, it is possible that the battery's SOC will reach 60% even under normal operating conditions. Therefore, 60% for the *SOC_Threshold* is used.

Based on the above discussions, the on-board computational procedure of the algorithm is as follows (see Figure 16 for a flow chart):

1) Obtain the battery voltage *V1* and *V2*;
2) Compute the voltage difference $\Delta V = V2 - V1$;
3) Use *EBT* to obtain *SOC_Threshold* and $\Delta V\_Threshold$ from the calibrated lookup table;
4) If $\Delta V < \Delta V\_Threshold$ and
   - *StartUpSOC* > *SOC_Threshold*, issue a message of "Replace Battery", return.
   - *StartUpSOC* ≤ *SOC_Threshold*, issue a message of "Recharge Battery", return.

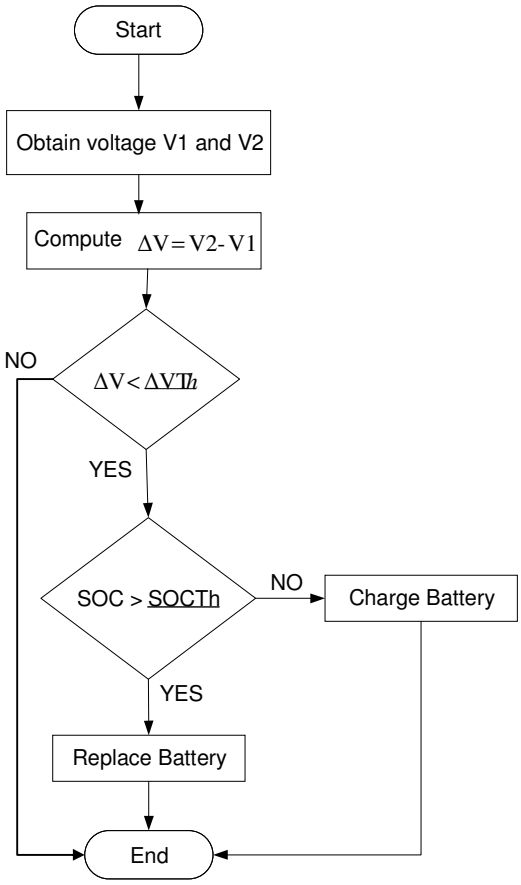

Figure 16: Flow chart of on-board implementation of battery SOH monitoring method.

To get more insight into the above procedure, let us consider two illustrative examples. If a battery at 25°C and 80% SOC has a ΔV = 0.2 (i.e., below the $\Delta V\_Threshold$), then a message of "Replace Battery" is issued. In contrast, a battery at 25°C and 20% SOC having ΔV = 0.2, would warrant a message of "Recharge Battery" based on the algorithm. Intuitively, in the former case, since the battery with 80% SOC has difficulty cranking the vehicle at 25°C, the battery should be replaced. For the latter, the battery's low cranking power could be due to low SOC (i.e., 20%), so the battery should first be recharged. In the following section, examples of the algorithm's performance evaluation results are presented in detail.

3.4 Algorithm Performance Evaluation

To evaluate the performance of the battery cranking voltage based method, the SOH monitoring algorithm described in Section 3.3 was applied to determine the SOH of 10 field batteries and 10 new Johnson Control (JCI) LN3 production batteries used to crank 2 vehicles under various conditions. The 10 field batteries were selected from a pool of approximately 100 field batteries collected from two distinct climate regions in the United States. The field batteries originated from dealer service garages in the Chicago, Illinois area and the Phoenix, Arizona area. These field batteries were tested at four different temperatures of 50°C, 25°C, 0°C, and -18°C. At each temperature, the batteries were first fully charged, and then the SOC was gradually reduced until it reached 0% SOC or the battery failed to crank the vehicle.

The 10 JCI LN3 batteries were aged through an accelerated aging process from fresh to end-of-life. Weekly vehicle cranking was conducted at high SOC (nearly 100%) and 25°C for each battery. Additionally, four batteries (JCI005, JCI006, JCI009, and JCI010) were pulled every 4 weeks to conduct vehicle test cranking at four different temperatures of -30°C, 0°C, 25°C, and 52°C and at different SOC levels.

Through extensive analysis of vehicle cranking data collected from field batteries and JCI LN3 production batteries aged through an accelerated aging process, the effectiveness of the cranking voltage based battery SOH monitoring algorithm has been extensively verified. As illustrative examples, two representative cases of the algorithm's performance evaluation results are presented at 25°C for field batteries in Section 3.4.1. In Section 3.4.2, an example of the algorithm's performance evaluation results for weekly cranking data collected from the 10 JCI LN3 batteries is presented.

Due to space limitations, only a few examples of the algorithm's evaluation results are presented in the following sections and throughout this thesis for each battery SOH monitoring algorithm. For more complete details of the algorithm's performance evaluation results for the battery cranking voltage based method, refer to [31].

3.4.1 Field Battery Cranking Data Evaluation Results

Two illustrative examples of the algorithm's performance evaluation results using the cranking data collected from 10 field batteries are presented in this section. The battery cranking voltage based SOH monitoring algorithm described in Section 3.3 was applied to determine the SOH of each battery. Each table shows the corresponding voltage differences, $\Delta V = V2 - V1$, generated for cranks at different SOC levels. The tables also indicate when the battery failed to crank the vehicle with the comment "failure". The values that are shaded are values below the $\Delta V\_Threshold$. As a reference, the results of this algorithm are compared with the output of the Midtronics Micro500XL battery tester. Each table is followed by comments on the data and performance of the SOH monitoring algorithm. In each table, the voltages are in volts.

- Field battery #69 and #42 cranked at 25°C and different SOC levels. The calibration values for *SOC_Threshold* and $\Delta V\_Threshold$ at 25°C are 60% SOC and 0.7 volts, respectively.

Table 2: Field battery #69 at 25°C.

SOC		100% SOC	90% SOC	80% SOC	75% SOC
crank #	1	1.156	1.294	0.914	**0.025**
	2	1.073	0.825	0.779	**-0.537**
	3	1.357	**0.628**	**0.306**	**failure**

Table 2 shows the results for battery #69 cranked 3 times four SOC levels: 100%, 90%, 80%, and 75%. Battery #69 failed to crank the vehicle at the third crank attempt of 75% SOC and at the next SOC level below 75%. Thus, this table is brief and includes only data from successful cranks including the first cranking failure at 75% SOC. Focusing on the data that is shaded, the algorithm determines that crank 3 at 90%, crank 3 at 80%, and all cranks at 75% SOC have a ΔV value below the threshold of 0.7 volts at 25°C. Moreover, the corresponding SOC of each of these cranks is higher than the 60% *SOC_Threshold*. This would warrant a message of "Replace Battery", which is consistent with the output from the Midtronics battery tester of "Replace Battery".

Table 3: Field battery #42 at 25°C.

SOC		100% SOC	90% SOC	80% SOC	75% SOC	70% SOC
crank #	1	1.117	1.192	1.447	1.267	1.088
	2	1.389	1.348	0.999	1.119	1.246
	3	1.184	1.315	1.127	1.114	1.029

SOC		65% SOC	60% SOC	55% SOC	50% SOC	45% SOC
crank #	1	0.975	1.177	0.887	0.871	**-0.473**
	2	0.996	1.182	1.267	**0.517**	**failure**
	3	1.235	1.258	1.094	0.755	**failure**

In Table 3, for battery #42, ΔV falls below the threshold (0.7) during crank 2 at 50% SOC and at crank 1 of 45% SOC. Then, the battery fails to crank during cranks 2 and 3 at 45% SOC. Therefore, the algorithm is capable of issuing a pre-warning message of "Recharge Battery" to avoid cranking failure. In contrast, the Midtronics battery tester issued a message of "Replace" which could result in unnecessary replacement of a good battery because of low SOC.

3.4.2 Weekly Cranking Data Evaluation Results

In this section, an example of the evaluation results from vehicle cranking data collected weekly throughout the accelerated aging process from one of the 10 JCI LN3 production batteries at high SOC (approximately 100%) and 25°C is presented. The battery cranking voltage based SOH monitoring algorithm described in Section 3.3 was applied to determine the SOH of each battery.

The Midtronics battery test was not conducted in this test. However, the testing vehicle was kept running for approximately thirty-five minutes to warm up the engine oil temperature to around 90°C before conducting the cranking test. Thus, the variation of engine conditions was reduced, and the cranking time is used as a reference of battery SOH to evaluate the effectiveness of the algorithm. It is worth noting that in real-world applications, cranking time is also sensitive to the conditions of other components of the starting system, for instance, the starter and the engine, therefore it cannot be directly used as a battery SOH indicator.

In the following table, each week is denoted as a test period and the last test period presented is one test period (one week) prior to cranking failure. The data included in the table reflects the battery's ΔV values and the engine cranking times for each crank at each test period. At 25°C, the calibration values for $\underline{\Delta V\_Threshold}$ and $\underline{SOC\_Threshold}$ are 0.7 volts and 60% SOC, respectively. Those ΔV values that are shaded are below the threshold. Thus, in the following analysis, when ΔV falls below 0.7 volts, the algorithm issues a recommendation to "Replace Battery", since 100% SOC is above the 60% SOC threshold. The cranking time for each crank is also presented in the

table as a reference of actual battery SOH to evaluate the effectiveness of the battery SOH monitoring algorithm.

Table 4: Battery JCI001 (high SOC at 25°C).

crank #	Test Period 1		Test Period 2		Test Period 3		Test Period 4	
	ΔV	crank time	ΔV	crank time	ΔV	crank time	ΔV	crank time
1	1.199	0.914	1.255	0.916	1.179	0.939	1.135	0.953
2	1.154	0.902	1.308	0.921	1.032	0.926	1.120	0.944
3	1.387	0.873	1.136	0.911	1.275	0.897	1.175	0.955

crank #	Test Period 5		Test Period 6		Test Period 7		Test Period 8	
	ΔV	crank time	ΔV	crank time	ΔV	crank time	ΔV	crank time
1	1.140	0.931	1.223	0.934	1.091	0.971	0.990	0.979
2	1.231	0.887	1.065	0.958	1.007	0.977	1.233	0.995
3	1.102	0.926	1.278	0.947	1.301	0.979	1.093	0.998

crank #	Test Period 9		Test Period 10		Test Period 11		Test Period 12	
	ΔV	crank time	ΔV	crank time	ΔV	crank time	ΔV	crank time
1	1.185	0.993	1.132	1.001	1.007	0.990	**0.096**	**1.143**
2	1.178	0.987	1.139	0.990	1.219	0.965	**-1.003**	**1.345**
3	1.068	0.926	1.064	0.980	1.025	0.989	**-1.263**	**1.758**

Table 4 shows the results for LN3 battery JCI001. The battery failed to crank the vehicle at test period 13. For test periods 1-11, all ΔV values are above the threshold of 0.7 and the corresponding crank times are approximately 1 second or less. This indicates that the battery has sufficient power to crank the engine. However, in test period 12, ΔV is below the 0.7 volts threshold for all three cranks, and the corresponding crank times are approximately 1.2 seconds or greater, which indicates that the battery's power capability is low. Based on the algorithm, a message of "Replace Battery" would be issued. Therefore, the algorithm provides a timely pre-warning before cranking failure at test period 13.

CHAPTER 4

PARITY-RELATION BASED SOH MONITORING METHOD

With the availability of battery sensors (e.g., from Bosch, Siemens, and Hella) that can accurately acquire the physical variables of the battery such as current, voltage, and temperature, a more robust diagnostic/prognostic technique to determine battery SOH by combining SOH indicators can be developed. Fusing battery SOH indicators enhances fault sensitivity and robustness to variations in battery type. This chapter describes a parity-relation (see, for example, [32][33][34]) based integrated approach to battery SOH monitoring method by using the battery voltage signal and high cranking current signal during vehicle starting. A parity-relation is defined to characterize the dynamics of good batteries during vehicle cranking. The parity-relation based SOH monitoring algorithm is refined and calibrated for real-time on-board implementation. The calibrated parity-relation can be used to estimate battery cranking voltage given a current signal. A residual, generated as the discrepancy between the actual voltage measurement and its estimation, is used to infer battery SOH. Through analysis of the residual based on the battery model during cranking discussed in Chapter 2, it is shown that the residual integrates the SOH information provided by both battery resistance and voltage loss, hence enhancing fault sensitivity and diagnostic/prognostic robustness.

Performance evaluation results using various vehicle cranking data collected from 20 batteries and 2 vehicles have shown the effectiveness of the algorithm.

This parity-relation based approach offers the same benefit as the battery cranking voltage based method, described in Chapter 3, by offering a pre-warning of battery end-of-life and avoid walk-home situations due to battery failures. Likewise, it can help to reduce battery no trouble found (NTF) and warranty cost.

The following sections describe the parity-relation based battery SOH monitoring method. Specifically, in Section 4.1, based on the new battery model developed in Chapter 2, the parity-relation based approached is analyzed to show its capability of integrating the SOH information provided by both battery resistance and voltage loss. In Section 4.2, an overview of the battery SOH monitoring method is provided. Section 4.4 details the residual generation. Section 4.4 gives a detailed description of the off-line calibration procedure and real-time on-board implementation of the SOH monitoring algorithm. Finally, Section 4.5 includes examples of the parity-relation based algorithm performance evaluation results through analysis of extensive vehicle cranking data collected from 10 field batteries and 10 JCI LN3 batteries.

4.1 Battery SOH Indicators

To perform effective fault diagnosis, features need to be extracted that are sensitive to faults. It is well known that battery resistance increases as a result of battery ageing [9]. However, to provide accurate and reliable battery diagnosis, the battery resistance needs to be combined with other features or methods via an integrated algorithm (e.g., [7][8]). In this research, it is found that voltage loss during cranking also

provides valuable information of battery SOH and can be used to enhance battery diagnosis and prognosis [35].

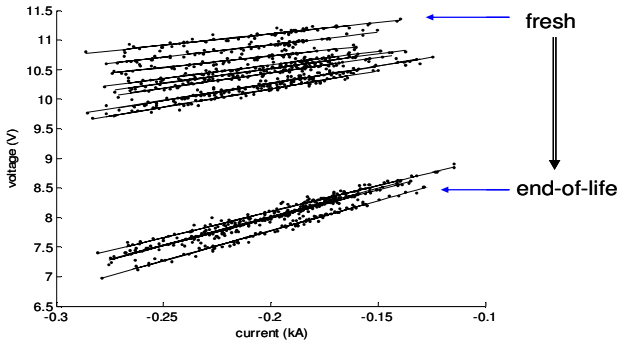

Figure 17: V-I plot of cranking data collected periodically during the complete accelerated ageing cycling process of a battery (the linear least squares fit line for each data set is also shown).

Figure 17 illustrates a few sets of cranking data collected periodically from a battery which was aged from fresh to end-of-life through accelerated ageing cycling. To minimize the effect of SOC variation, the battery was always kept at a high SOC level of about 90%, when vehicle test cranking was conducted. For simplicity, only the data samples with battery current in the range of -300A to -100A are shown in Figure 17. For the data collected during each cranking, the linear least squares fit line is also shown.

The battery resistance R and voltage loss V_{loss} for each set of cranking data are extracted based on (18) and (19). As shown in Figure 18 and Figure 19, both battery resistance and voltage loss have a general trend of increasing during the ageing process. These two SOH indicators can be integrated to improve the performance of the fault diagnostic/prognostic scheme, which motivates the proposed battery SOH monitoring method.

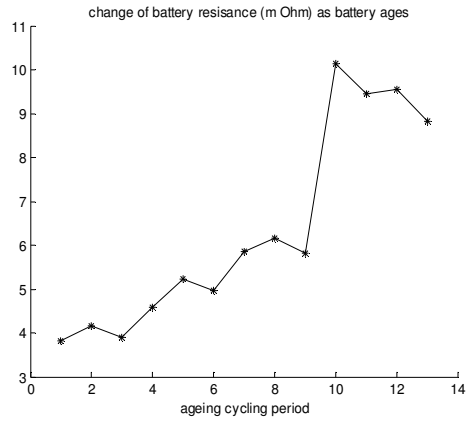

Figure 18: Battery resistance in a complete accelerated ageing cycling process.

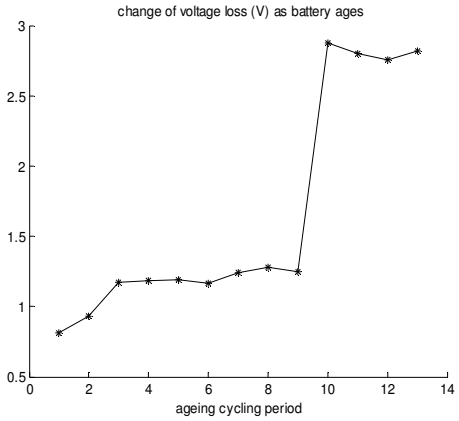

Figure 19: Battery voltage loss in a complete accelerated ageing cycling process.

4.2 Parity-Relation Based Battery SOH Monitoring Method

Figure 20 illustrates a schematic diagram of the parity-relation based battery SOH monitoring method. It consists of the following four components:

- ***Signal preprocessing***. The battery voltage and current signals are preprocessed to extract the portion of signals corresponding to the short period of engine cranking.
- ***Voltage estimation***. A trained parity-relation model, characterizing the dynamics of good batteries during engine cranking, is used to generate an estimation of the battery voltage, given a battery current signal.
- ***Residual generation***. The residual is defined as the discrepancy between the actual voltage measurement and its estimated value provided by the trained parity-relation. Based on our design, the residual is designed such that it remains greater than or around zero for good batteries, and takes significant negative values for bad batteries.

- ***Residual evaluation***. By comparing the diagnostic residual with a calibrated threshold, the battery SOH is inferred. The effects of battery SOC and temperature should be taken into account during the residual evaluation process.

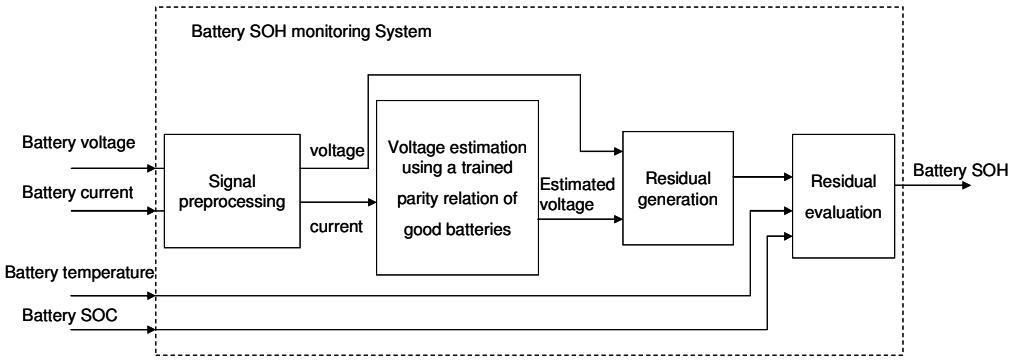

Figure 20: Parity-relation based battery SOH monitoring method.

Fault sensitivity and robustness to modeling errors are two very important performance metrics of fault diagnostics/prognostics. In general, the sensitivity and robustness properties can be enhanced either during residual generation or during residual evaluation [32][33][34]. In this research, the former approach was chosen. More specifically, residual generation is designed to combine the SOH utilizing battery resistance and SOH utilizing voltage loss, hence achieving better sensitivity and robustness. It is computationally efficient since it doesn't require real-time identification of battery model parameters [25]. Next, the details of residual generation are described.

4.3 Residual Generation

The discrepancy between the actual voltage and the estimated voltage measurement is defined as the diagnostic residual, which intuitively characterizes the deviation between

the behavior of the battery under consideration and that of good batteries. Specifically, the diagnostic residual $r(t)$ is defined in (23), where $\hat{V}(t)$ is the estimated voltage generated by (24).

$$r(t) = V(t) - \hat{V}(t), \tag{23}$$

$$\hat{V}(t) = \underline{V}_0 + I(t) * \underline{R}_b. \tag{24}$$

The calibration parameters $\underline{V}_0$ and $\underline{R}_b$ are obtained based on (19) using data collected from good batteries (see Section 4.4.1 for more details).

As described above, a unique feature of the residual $r(t)$ is that it combines the battery SOH information provided by both battery resistance and voltage loss. The following analysis gives a better insight into the design of residual, $r(t)$. By using (22), the measured battery voltage $V(t)$ satisfies (25), where V_{ocv}, V_{loss}, and R_b characterizes the properties of the battery under testing.

$$V(t) = V_{ocv} - V_{loss} + I(t) * R_b, \tag{25}$$

By substituting (24) and (25) into (23), we have

$$\begin{aligned} r(t) &= V_{ocv} - \underline{V}_0 - V_{loss} - I * (\underline{R}_b - R_b) \\ &= (V_{ocv} - \underline{V}_{ocv}) + (\underline{V}_{loss} - V_{loss}) - I * (\underline{R}_b - R_b) \end{aligned} \tag{26}$$

Since $V_{ocv} \approx \underline{V}_{ocv}$ at the same battery SOC and temperature, equation (26) can be further simplified as (27), where $I(t) < 0$ for discharge.

$$r(t) = (\underline{V}_{loss} - V_{loss}) - I * (\underline{R}_b - R_b), \tag{27}$$

As shown in Figure 18 and Figure 19, the battery voltage loss and internal resistance will both increase as a result of battery ageing. Therefore, the residual $r(t)$ given by (27) combines the changes of both battery voltage loss and internal resistance as a result of battery aging, hence improving diagnostic sensitivity and robustness. More specifically, the residual will remain positive or near zero for good batteries since $\underline{V}_{loss} \approx V_{loss}$ and $\underline{R}_b \approx R_b$ and become increasingly negative when either V_{loss} and/or R_b increase as a result of battery aging. Therefore, the residual $r(t)$ has better diagnostic performance than conventional methods that are solely based on battery resistance.

It is worth noting that, since the battery voltage and current have a linear relationship during vehicle cranking (see, e.g., Figure 4), for the simplicity of implementation, we can apply (25) only to battery voltage and current data samples with a cranking current in the range of -300A < I < -100A. Moreover, to minimize the effect of noise and disturbance, the residual is filtered by taking its average for each cranking data set. Specifically, assume there are n data samples satisfying -300A < I < -100A in one cranking data set, the filtered residual is given by (28).

$$r = \frac{1}{n}\sum_{i=1}^{n} r(i). \tag{28}$$

The diagnostic residual is evaluated using calibrated residual threshold values, obtained based on the analysis of extensive vehicle cranking data collected from a variety of batteries. Next, the details of the off-line calibration procedure and the on-board implementation of the battery SOH monitoring algorithm will be discussed.

4.4 Off-line Calibration and On-board Implementation of the SOH Monitoring Algorithm

The parity-relation based method implicitly combines the SOH information provided by battery resistance and voltage loss during cranking, hence achieving better diagnostic performance. It is computationally efficient since it doesn't require real-time identification of battery model parameters. Next, details of the off-line calibration procedure and on-board implementation of the proposed battery SOH monitoring algorithm are discussed.

4.4.1 Off-line Parity-Relation Calibration Procedure

An off-line calibration procedure is performed to obtain a parity-relation model characterizing the dynamics of good batteries during cranking at different SOC levels and temperatures. Specifically, to determine the calibration parameters $\underline{V}_0$ and $\underline{R}_b$ in (24), the following steps are carried out.

1) Perform cranking tests using selected good batteries, and collect the battery voltage $V(t)$ and current $I(t)$ at a sampling period of 50ms for 1 second during cranking.

2) Conduct a linear regression in the form of (29), where $\underline{V}_0$ is the intercept voltage (i.e., voltage at $I = 0$) of the linear regression line, and $\underline{R}_b$ is the slope of the linear regression line (see Figure 21). Record the parameters $\underline{V}_0$ and $\underline{R}_b$.

$$V(t) = \underline{V}_0 + I(t) * \underline{R}_b, \tag{29}$$

3) Repeat steps 1 and 2 at different battery SOC levels (e.g., 100%, 75%, 50%, 25%) and temperatures (e.g., 50°C, 25°C, 0°C, -18°C).

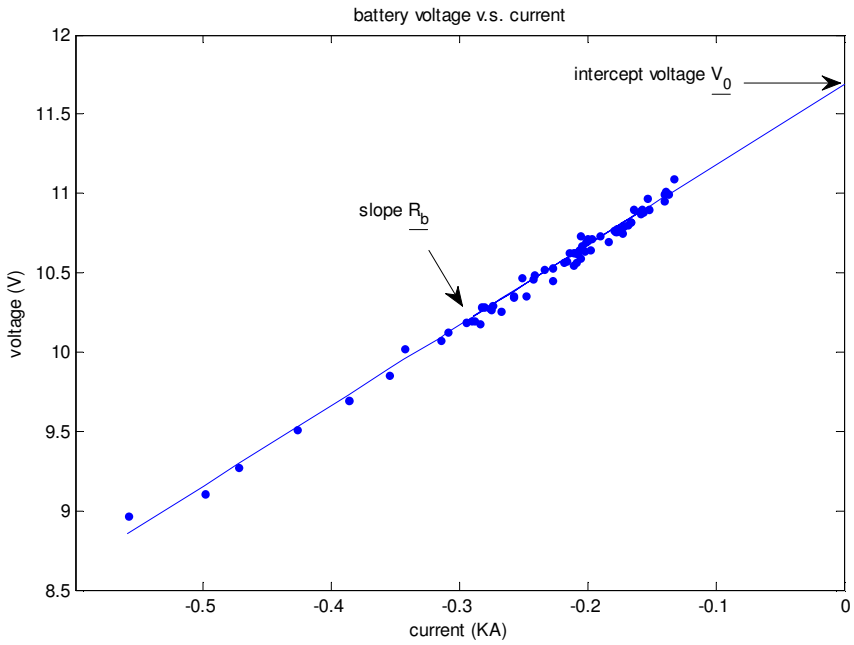

Figure 21: Linear regression line of extracted battery voltage and current signals.

The parameters obtained from the off-line calibration are then stored in a 4x4, 2-D look-up table and can be used to generate an estimation of battery voltage, $\hat{V}(t)$, given any battery current signal using (24) for on-board vehicle applications.

4.4.2 On-board Implementation

In this section, details are provided for the on-board implementation procedure of this proposed battery SOH monitoring algorithm. The inputs to the algorithm are the battery voltage and current at a sampling period of 50ms for 1 second, battery start-up SOC, and battery temperature. The specifications of the sensor signals and variables are listed in Table 5.

Table 5: Specifications of sensor signals and variables.

Battery signals	accuracy	resolution	range	# of samples	sampling rate
Current (A)	+/- 5	0.1	-1200 to +200	20	50ms
Voltage (V)	+/- 0.1	0.001	0 to 16	20	50ms
Temperature (0C)	+/- 5	1	-40 to +80	1	1 sample
SOC (%)	+/- 10	1	0 to 100	1	1 sample

In addition to the calibration parameters $\underline{V}_0$ and $\underline{R}_b$ described in Section 4.4.1, the proposed on-board implementation of the algorithm has two other calibration parameters:

- A threshold *SOC_Threshold* calibrated as a 1x4 2-D look-up table as a function of *EBT* (estimated battery temperature) (e.g., 50°C, 25°C, 0°C, -18°C).
- A residual threshold $\underline{r}$ calibrated as a 1x4 2-D look-up table as a function of *EBT* (e.g., 50°C, 25°C, 0°C, -18°C).

It is worth noting that a negative constant for $\underline{r}$ is used. Note that a good battery will have $V(t)$ values greater or close to $\hat{V}(t)$ values. Thus, the residual, *r*, will be positive or near zero. In contrast, an aged battery will have sample $V(t)$ values less than the estimated voltages $\hat{V}(t)$. Thus, obtaining the residual by subtracting $\hat{V}(t)$ from $V(t)$ will result in negative residual values (see equation (23)).

Moreover, low battery cranking power can be caused by low battery SOH and/or low SOC. To determine if a battery should be replaced or charged to ensure the vehicle's start-up ability, the following method is adopted:

- If the residual is below its threshold, and battery SOC is above a certain calibrated level, then the battery should be replaced.
- If the residual is below its threshold, and battery SOC is below a certain calibrated level, then the battery is first recharged.

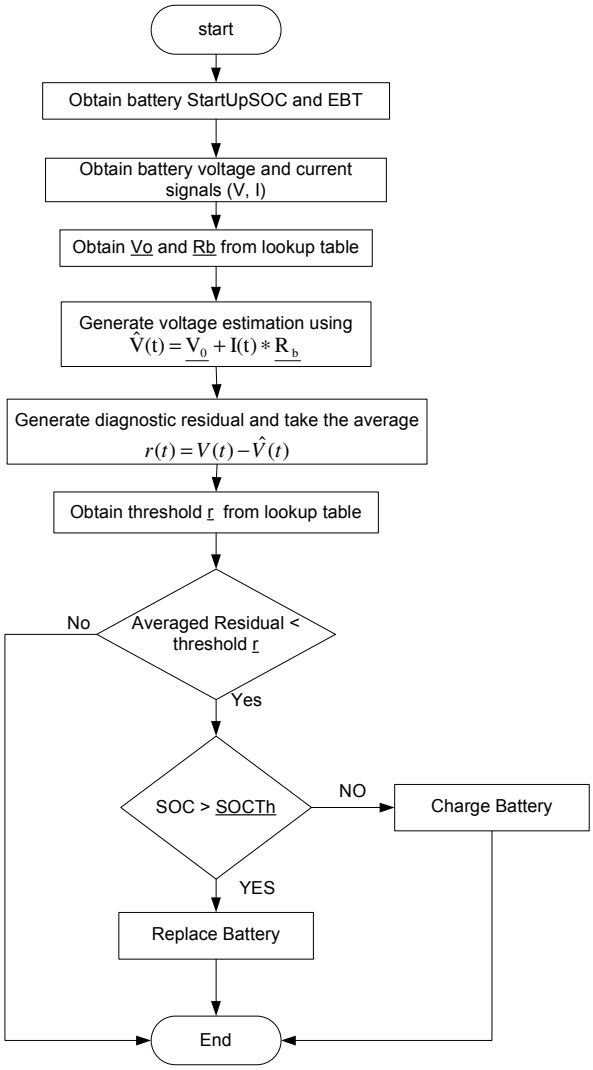

Figure 22: Flow chart for the on-board computational procedure.

Based on the above discussions, a detailed on-board computational procedure of the SOH monitoring method is shown in Figure 22 and described in the following steps:

1) Obtain the battery *StartUpSOC* and temperature (*EBT*);
2) Measure battery voltage $V(t)$ and current $I(t)$ at a sampling period of 50 ms for 1 second during cranking;
3) Based on battery *StartUpSOC* and *EBT*, obtain $\underline{V}_0$ and $\underline{R}_b$ from the lookup tables;

4) For each $I(t)$, compute a voltage estimation as $\hat{V}(t) = \underline{V}_0 + I(t) * \underline{R}_b$;

5) Compute the 20 samples of residual $r(t) = V(t) - \hat{V}(t)$, and take the average of the residual signal $r(t)$ to obtain r;

6) Use *EBT* to obtain a threshold on residual $\underline{r}$ and *SOC_Threshold* from the calibrated lookup table;

7) If $r < \underline{r}$ and

   a. *StartUpSOC* > *SOC_Threshold*, issue a message of "Replace Battery", return.

   b. *StartUpSOC* ≤ *SOC_Threshold*, issue a message of "Recharge Battery", return.

To get more insight into the above procedure, let us consider two illustrative examples. If a battery at 25°C and 80% SOC has an r = -1.3 (i.e., below the $\underline{r}$ *Threshold*), then a message of "Replace Battery" is issued. In contrast, a battery at 25°C and 20% SOC having r = -1.3, would warrant a message of "Recharge Battery" based on the algorithm. Intuitively, in the former case, since the battery with 80% SOC has difficulty cranking the vehicle at 25°C, the battery should be replaced. For the latter, the battery's low cranking power could be due to low SOC (i.e., 20%), so the battery should first be recharged. In the following section, examples of the algorithm's performance evaluation results are presented in detail.

4.5 Algorithm Performance Evaluation

To evaluate the performance of the parity-relation based method, the SOH monitoring algorithm described in Section 4.4 was applied to determine the SOH of 10 field batteries and 10 JCI LN3 production batteries used to crank 2 vehicles under various conditions. Through extensive analysis of vehicle cranking data collected from field batteries and JCI LN3 production batteries aged through an accelerated aging process, the effectiveness of the parity-relation based battery SOH monitoring algorithm has been extensively verified. As illustrative examples, two representative cases are presented at 25°C for field batteries in Section 4.5.1. In Section 4.5.2, an example of the algorithm's performance evaluation results for weekly battery cranking data collected from the 10 JCI LN3 batteries is presented.

Due to space limitations, only a few examples of the algorithm's evaluation results are presented in the following sections. For more complete details of the algorithm's performance evaluation results for the parity-relation based method, refer to [36].

4.5.1 Field Battery Residual Evaluation Results

Two illustrative examples of the evaluation results of residuals generated from vehicle cranking data collected from 10 field batteries at 25°C are presented in this section. All field batteries were tested at four different temperatures of 50°C, 25°C, 0°C, and -18°C. At each temperature, the batteries were first fully charged, and then the SOC was gradually reduced until it reached 0% SOC or the battery failed to crank the vehicle.

The parity-relation based SOH monitoring algorithm described in Section 4.4 was applied to determine the SOH of each battery. Each table shows the corresponding residual values, for vehicle cranking at different SOC levels. The tables also indicate when the battery failed to crank the vehicle with the comment "failure". The values that are shaded are values below the residual threshold. As a reference, the results of this algorithm are compared with the output of the Midtronics Micro500XL battery tester. Each table is followed by comments on the data and performance of the SOH monitoring algorithm. In each table, the residual values are in volts.

- Batteries #69 and #42 cranked at 25°C and different SOC levels. The calibration values for *SOC_Threshold* and *r_Threshold* at 25°C are 60% SOC and -1.2 volts, respectively.

Table 6: Field battery #69 at 25°C.

SOC		100% SOC	90% SOC	80% SOC	75% SOC
crank #	1	-1.136	**-1.518**	**-2.055**	**-2.532**
	2	**-1.231**	**-1.723**	**-2.351**	**-3.110**
	3	**-1.283**	**-1.858**	**-2.414**	**failure**

Reported in Table 6 are the results for battery #69 cranked 3 times at each of four SOC levels: 100%, 90%, 80%, and 75%. The battery failed to crank the vehicle at the third attempt of 75% SOC and at the next SOC level below 75% SOC. Focusing on the data that is shaded, the algorithm determines that the second and third cranks at the 100% SOC level and all cranks thereafter have a residual value below the threshold of -1.2 at 25°C. Moreover, the corresponding SOC of each of these cranks is higher than the 60% *SOC_Threshold*. This would warrant a message of "Replace Battery". This message is consistent with the message issued from the Midtronics battery tester of "Replace Battery".

Table 7: Field battery #42 at 25°C.

SOC		100% SOC	90% SOC	80% SOC	75% SOC	70% SOC
crank #	1	-0.003	-0.097	-0.226	-0.359	-0.422
	2	0.019	-0.138	-0.305	-0.413	-0.464
	3	0.049	-0.143	-0.337	-0.406	-0.432

SOC		65% SOC	60% SOC	55% SOC	50% SOC	45% SOC
crank #	1	-0.459	-0.607	-0.792	**-1.304**	**-2.745**
	2	-0.514	-0.668	-0.889	**-1.542**	**failure**
	3	-0.508	-0.689	-0.918	**-1.759**	**failure**

Table 7 reports the results for battery #42. The battery fails to crank the vehicle during cranks 2 and 3 at 45% SOC and the next SOC level below 45% SOC. The residual values fall below the threshold of -1.2 at 50% SOC and thereafter. Thus, the algorithm is capable of issuing a pre-warning message of "Recharge Battery" to avoid cranking failure at 45% SOC. The Midtronics battery tester outputs a message of "Replace Battery", which could result in unnecessary replacement of a good battery.

4.5.2 Residual Evaluation Results for JCI LN3 Batteries Tested Weekly

In this section, an example of the evaluation results of residuals generated from vehicle cranking data collected weekly throughout the accelerated aging process from 10 JCI LN3 production batteries at high SOC (approximately 100%) and 25°C is presented. The 10 batteries were aged using accelerated aging procedures from fresh to end-of-life. Weekly vehicle cranking was conducted at high SOC and 25°C for each battery. The parity-relation based SOH monitoring algorithm described in Section 4.4 was applied to determine the SOH of each battery.

The Midtronics battery test was not conducted in this test. However, the testing vehicle was kept running for approximately thirty-five minutes to warm up the engine oil temperature to around 90^{o}C before conducting the cranking test. Thus, the variation of engine conditions was reduced, and the cranking time is used as a reference of battery SOH to evaluate the effectiveness of the algorithm. It is worth noting again, that in real-world applications, cranking time is also sensitive to the conditions of other components of the starting system, for instance, the starter and the engine, therefore it cannot be directly used as a battery SOH indicator.

In the following tables, each week is denoted as a test period and the last test period is one test period (one week) prior to cranking failure. The data included in the table reflects the residual values and cranking time for each crank at each test period. At 25°C, the calibration values for *r Threshold* and *SOC_Threshold* are -1.2 volts and 60% SOC, respectively. Those residual values that are shaded are below the threshold. Thus, in the following analysis, when the residual value falls below -1.2 volts, the algorithm issues a recommendation to "Replace Battery", since 100% SOC is above the 60% SOC threshold. As described above, the cranking time can be used as a reference of actual battery SOH to evaluate the effectiveness of this battery SOH monitoring algorithm. Additionally, in the following tables, residual cells with the remark "bad data" indicate that the collected current data, $I(t)$, was corrupted. Thus, the residual values for those cranks cannot be calculated.

Table 8: Battery JCI002 (high SOC at 25°C).

crank #	Test Period 1		Test Period 2		Test Period 3		Test Period 4	
	residual	crank time	residual	crank time	residual	crank time	residual	crank time
1	0.478	0.922	0.335	0.925	0.086	0.925	-0.029	0.948
2	0.459	0.885	0.364	0.870	0.121	0.918	-0.026	0.944
3	0.469	0.894	0.371	0.905	0.126	0.925	-0.014	0.933

crank #	Test Period 5		Test Period 6		Test Period 7		Test Period 8	
	residual	crank time	residual	crank time	residual	crank time	residual	crank time
1	-0.158	0.941	-0.247	0.947	-0.399	0.986	-0.322	0.983
2	-0.159	0.963	-0.223	0.959	-0.361	1.000	-0.308	0.983
3	-0.160	0.955	-0.247	0.971	-0.363	0.988	-0.337	1.002

crank #	Test Period 9		Test Period 10	
	residual	crank time	residual	crank time
1	bad data	1.017	**-2.382**	**1.198**
2	bad data	1.015	**-2.682**	**1.308**
3	bad data	1.054	**-2.635**	**1.310**

Table 8 shows the results for battery JCI002. The battery failed to crank the vehicle at test period 11. For test periods 1-8, the residual values are above the threshold of -1.2 volts and the corresponding crank times are approximately 1 second or less. This indicates that the battery has sufficient power to crank the engine. The residuals for test period 9 cannot be calculated due to corrupted current signals. During test period 10, the residual values are well below the threshold of -1.2. Thus, the algorithm issues a timely pre-warning of "Replace Battery" at test period 10 to avoid cranking failure at test period 11. Note that the crank times in the shaded cells are approximately 1.2 seconds or greater (vs. less than 1 second at normal conditions), indicating low SOH.

CHAPTER 5
COMPARATIVE STUDIES

In this chapter, comparative studies are conducted to further evaluate the performance, cost, and benefits of the battery SOH monitoring algorithms. First, the conventional resistance based approach is compared to the two battery SOH monitoring methods covered in Chapter 3 and Chapter 4. The weakness of the conventional resistance based method with respect to variation of battery types is discussed, and the robustness of the battery cranking voltage based approach and the parity-relation based approach, in determining battery SOH for different types of batteries, is demonstrated. Furthermore, the battery cranking voltage based approach is compared with the parity-relation based approach to analyze the benefit with the use of an additional cranking current sensor.

This chapter is organized as follows. Section 5.1 provides an overview of the conventional resistance based battery SOH monitoring method. Section 5.2 presents a comparison of the two SOH monitoring methods developed in chapters 3 and 4 with the conventional resistance based method. Section 5.3 and Section 5.4 present a comparison between the battery cranking voltage based method and the parity-relation based method using examples from extensive vehicle cranking data collected from 10 field batteries and 10 JCI LN3 production batteries, respectively.

5.1 Conventional Resistance Based Method

The basic idea of the resistance based approach consists of three steps. First, we pre-process the battery voltage and current signals by extracting the terminal voltages corresponding to two specific current loads. Second, using the voltage and current values extracted during signal pre-processing, the internal resistance, comprised of the ohmic resistance within the electrodes and electrolyte, can be determined using Ohm's law [11]. Finally, with additional information of the battery SOC and temperature, a resistance threshold can be calibrated to infer battery SOH.

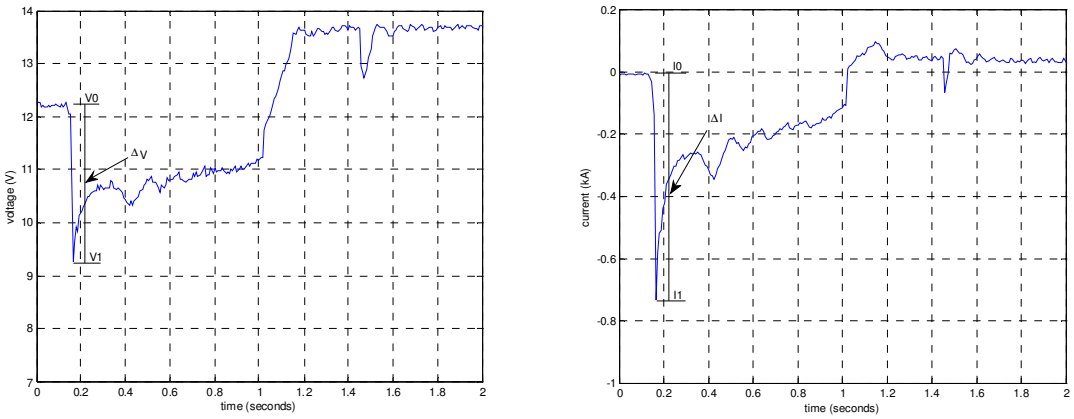

Figure 23: Voltage and current plots illustrating the calculation of resistance.

The variables used to calculate the battery resistances from each crank data set are illustrated in Figure 23. More specifically, ΔV is the voltage difference between V_1 (i.e., the minimum voltage recorded at the instant of starter engagement) and V_0 (i.e., the voltage just prior to starter engagement). The current change, ΔI, is the difference between I_1 (i.e., the maximum current corresponding to V_1 at the instant of starter

engagement) and I_0 (i.e., the current corresponding to V_0 recorded just prior to starter engagement). Then, the battery cranking resistance can be computed using (30).

$$R = \frac{\Delta V}{\Delta I} = \frac{V_1 - V_0}{I_1 - I_0}. \tag{30}$$

5.2 Comparison with Conventional Resistance Based SOH Monitoring Method

This section presents comparative results between the conventional resistance based SOH monitoring method and the two previous methods developed in the research work, including the battery cranking voltage base method and the parity-relation based method. The three SOH monitoring algorithms were applied to analyze the SOH of 30 batteries to compare their performances. Specifically, 20 JCI LN3 batteries aged by an accelerated aging procedure and 10 field batteries collected from dealer service garages are considered.

Next, the battery data collected at 25°C is used as illustrative examples to show the advantage and disadvantages of these three SOH monitoring methods in terms of robustness to variation of battery types. The *ΔV_Threshold* for the cranking voltage based method and *r Threshold* for the parity-relation based method at 25°C is 0.7 volts and -1.2 volts, respectively, and the *SOC_Threshold* is 60% for both.

Table 9 shows the results for the calculated battery resistance (R), ΔV values, and residual values, *r*, for battery JCI006, respectively, at an SOC level higher than 90% SOC

and 25°C. The data was collected weekly throughout an accelerated aging process. The last test period presented is one test period (one week) prior to cranking failure. In each table, ΔV values and residual values, r, are in volts, and resistance values, (R), are in milliohms. Additionally, in the following tables, the remark "bad data" indicates that the collected current data $I(t)$ was corrupted. Thus, the resistance and residual values for those cranks could not be calculated.

In the following comparative analysis, when ΔV falls below 0.7 volts or r falls below -1.2 volts, the cranking voltage based method and the parity-relation based method issue a recommendation of "Replace Battery", respectively, since 90% SOC is above the 60% SOC threshold. The ΔV values and residual values that are below their corresponding thresholds are highlighted in gray.

Table 9: Battery JCI006 (high SOC at 25°C).

test period	R	ΔV	*r*
1	3.240	0.998	0.200
	3.338	1.095	0.206
	3.356	1.076	0.217
2	3.518	1.217	0.075
	3.231	1.065	0.115
	3.529	1.331	0.145
3	3.687	1.078	0.052
	3.644	1.043	0.095
	3.671	1.068	0.126
4	bad data	1.170	bad data
	bad data	1.077	bad data
	bad data	1.126	bad data
5	3.649	1.035	0.007
	3.950	1.318	0.009
	3.949	1.283	0.026
6	3.906	1.100	-0.018
	3.676	1.118	0.056
	3.925	1.169	0.052
7	3.991	1.119	-0.072
	4.075	1.218	0.008
	4.007	1.121	0.002
8	3.995	1.103	-0.087
	3.986	1.053	-0.009
	3.921	1.049	-0.001
9	4.097	1.066	-0.156
	4.393	1.220	-0.140
	4.341	1.198	-0.130
10	3.841	0.987	0.031
	3.647	0.888	0.027
	3.891	1.071	0.026
11	4.107	1.063	0.012
	3.921	0.993	0.067
	4.073	1.094	0.069
12	4.864	1.214	-0.266
	4.886	1.178	-0.152
	4.653	1.180	-0.135
13	4.768	**-0.314**	**-1.433**
	4.997	**-0.327**	**-1.628**
	5.362	**-0.420**	**-1.871**

Battery JCI006 failed to crank the vehicle at test period 14 (week 14). From resistance values shown in Table 9, a resistance threshold of about 4.9 milliohms might be chosen to provide a pre-warning of pending cranking failure at test period 14 for battery JCI006.

To get further insight into the battery resistance data in Table 9, the battery cranking voltage signals for battery JCI006 at the first week and the last week of the accelerated aging process and the corresponding V-I plots are illustrated in Figure 24. As can be seen in Table 9, the battery resistance values increase only slightly from week 1 to week 13. This is due in part to *V1*, the minimum cranking voltage at the instant of starter engagement, changing slightly from week 1 to week 13. Thus, in equation (30), ΔV and consequently the resistance would have a small change.

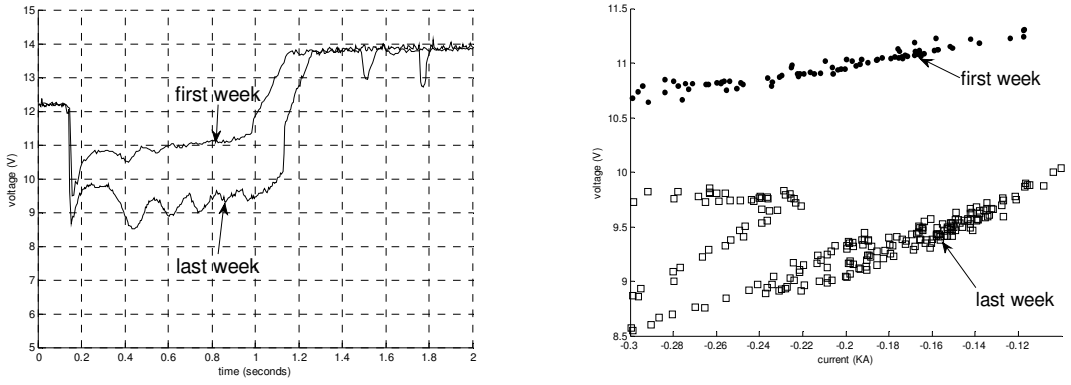

Figure 24: Battery cranking voltage signals and corresponding V-I plots from battery JCI006.

A key challenge of on-board battery SOH monitoring is robustness to variation of battery types. The driver may install any kind of after-market battery on the vehicle, which has to be taken into account in real-world battery SOH monitoring applications. In

addition to the 10 JCI LN3 batteries aged by GM, 20 other batteries to evaluate algorithm robustness have been considered.

Table 10: TAWAS aging data batteries #1 to #10 at first week (high SOC at 25°C).

Battery #	R	ΔV	r
1	7.010	1.761	0.114
2	6.881	1.664	0.142
3	6.918	1.767	0.109
4	6.847	1.804	0.112
5	6.902	1.579	0.137
6	6.615	1.705	0.463
7	6.534	1.782	0.486
8	6.481	1.836	0.473
9	6.639	1.772	0.470
10	6.548	1.819	0.453

Table 10 shows the calculated battery resistance (R), ΔV values, and residual values, r, for another set of 10 fresh JCI LN3 batteries. These fresh batteries were cranked at high SOC and 25°C. As can be seen in Table 10, these fresh batteries have a battery resistance of about 6.8 milliohms. As in the example of battery JCI006 shown in Table 9, if only resistance was used to determine battery SOH with a threshold of 4.9 milliohms, all these fresh batteries will be mistakenly determined as bad batteries and replaced. In contrast, the ΔV and residual values are well above their corresponding thresholds, indicating good battery SOH. Hence, the voltage based method and parity-relation based method are more robust than the conventional resistance based method.

Furthermore, Table 11 and Table 12 show the calculated battery resistances for all SOC levels presented and the ΔV and residual values for 100%, 90%, and 80% SOC of two field batteries cranked at different SOC levels at 25°C. These batteries were first fully charged, and then the SOC was gradually reduced until the batteries failed to crank the vehicle.

Table 11: Field battery #38 at 25°C.

SOC		100% SOC			90% SOC			80% SOC		
		R	ΔV	r	R	ΔV	r	R	ΔV	r
crank #	1	5.117	1.322	0.074	5.580	1.310	0.010	5.484	1.231	-0.065
	2	5.205	1.232	0.073	5.541	1.452	-0.007	5.339	1.249	-0.074
	3	5.295	1.433	0.099	5.637	1.326	0.005	5.294	1.143	-0.063

SOC		75% SOC	70% SOC	65% SOC	60% SOC	55% SOC	50% SOC	45% SOC	40% SOC	35% SOC
		R	R	R	R	R	R	R	R	R
crank #	1	5.653	5.651	5.607	5.774	5.566	6.303	6.262	9.120	9.968
	2	5.509	5.458	5.540	5.637	5.626	6.250	6.239	9.334	9.705
	3	5.419	5.562	5.537	5.670	5.676	6.185	6.017	9.547	9.980

SOC		30% SOC	25% SOC
		R	R
crank #	1	11.027	11.709
	2	10.154	12.919
	3	10.305	13.240

Table 12: Field battery #42 at 25°C.

SOC		100% SOC			90% SOC			80% SOC		
		R	ΔV	r	R	ΔV	r	R	ΔV	r
crank #	1	5.402	1.117	-0.003	5.937	1.192	-0.097	6.228	1.447	-0.226
	2	5.601	1.389	0.019	5.963	1.348	-0.138	6.075	0.999	-0.305
	3	5.704	1.184	0.049	6.018	1.315	-0.143	5.981	1.127	-0.337

SOC		75% SOC	70% SOC	65% SOC	60% SOC	55% SOC	50% SOC	45% SOC
		R	R	R	R	R	R	R
crank #	1	6.325	6.447	6.976	7.375	8.238	10.121	12.728
	2	6.248	6.532	6.777	7.552	8.214	10.474	failure
	3	6.253	6.364	6.837	7.440	8.396	11.041	failure

In Table 11, battery #38 failed to crank the vehicle at the next SOC level below 25% SOC. In Table 12, battery #42 failed to crank the vehicle at the 2nd and 3rd cranks of 45% SOC and at the next SOC level below. If a battery resistance based SOH monitoring method was employed for these two batteries using a resistance threshold of 4.9 milliohms to pre-warn of pending cranking failure, these two field batteries, at high SOC (i.e., 100% and 90% SOC), would be mistakenly determined as bad batteries and replaced. In contrast, the ΔV and residual values are well above threshold at 100% to

80% SOC, indicating good battery SOH. Again, the voltage based method and parity-relation based method are more robust than the conventional resistance based method.

Based on the above discussions, the battery cranking voltage and parity-relation methods are more robust to variation of battery types. This is crucial to on-board automotive battery SOH monitoring, since there is no control over the types of battery the vehicle owner may install on the vehicle.

5.3 Comparison of SOH Monitoring Methods

This section describes the comparison of the battery cranking voltage based method with the parity-relation based method of SOH monitoring for batteries obtained from the field and JCI LN3 production batteries. The SOH monitoring algorithms described in Section 3.3 and Section 4.4, respectively, were applied to determine the SOH of each battery.

Illustrative examples of the comparison of the two SOH monitoring methods for field batteries and JCI LN3 batteries tested weekly are presented in the Section 5.3.1, Section 5.3.2, respectively, including comparative analyses of the algorithms' performance evaluation results. Again, due to space limitations, only a few examples of the comparative evaluation results are presented. For more results, refer to [37].

5.3.1 Comparison of SOH Monitoring Methods Using Field Batteries

This section describes the comparison of the battery cranking voltage based method with the parity-relation based method for SOH monitoring for 10 batteries

obtained from the field. The batteries were tested at temperatures of 50°C, 25°C, 0°C, and -18°C. At each temperature, the batteries were first fully charged, and then the SOC was gradually reduced until it reached 0% SOC or the battery failed to crank the vehicle. The SOH monitoring algorithms described in Section 3.3 and Section 4.4 were applied to determine the SOH of each battery.

Below, illustrative examples are presented that represent a comparison of the SOH monitoring algorithms using ΔV and residual values generated from vehicle cranking data collected from field batteries at 25°C. Each table shows the corresponding ΔV and residual values for cranks at different SOC levels. The tables also indicate when the battery failed to crank the vehicle with the comment "failure". The values that are shaded are values below the (*ΔV_Threshold*) and (*r Threshold*). As a reference, the results of the algorithms are compared with the output of the Midtronics Micro500XL battery tester.

- Comparison of batteries #42 and #69 cranked at 25°C and different SOC levels. The calibration values for *ΔV_Threshold*, *r Threshold*, and *SOC_Threshold* at 25°C are 0.7 volts, -1.2 volts, and 60% SOC, respectively.

Table 13: Field battery #42 at 25°C.

SOC		100% SOC		90% SOC		80% SOC		75% SOC		70% SOC	
		ΔV	r	ΔV	r	ΔV	r	ΔV	r	ΔV	r
crank #	1	1.117	-0.003	1.192	-0.097	1.447	-0.226	1.267	-0.359	1.088	-0.422
	2	1.389	0.019	1.348	-0.138	0.999	-0.305	1.119	-0.413	1.246	-0.464
	3	1.184	0.049	1.315	-0.143	1.127	-0.337	1.114	-0.406	1.029	-0.432

SOC		65% SOC		60% SOC		55% SOC		50% SOC		45% SOC	
		ΔV	r	ΔV	r	ΔV	r	ΔV	r	ΔV	r
crank #	1	0.975	-0.459	1.177	-0.607	0.887	-0.792	0.871	**-1.304**	**-0.473**	**-2.745**
	2	0.996	-0.514	1.182	-0.668	1.267	-0.889	**0.517**	**-1.542**	**failure**	**failure**
	3	1.235	-0.508	1.258	-0.689	1.094	-0.918	0.755	**-1.759**	**failure**	**failure**

Table 13 reports the comparative results for battery #42. The battery fails to crank the vehicle during cranks 2 and 3 at 45% SOC and the next SOC level below 45% SOC. The ΔV and residual values fall below their respective thresholds at 50% SOC and thereafter. Thus, both of the algorithms are capable of issuing a pre-warning message of "Recharge Battery" to avoid crank failure at 45%. Moreover, looking at the residual values for 50% SOC, the parity-relation based method is more consistent in the sense that, once the residual value falls below the threshold during crank 1, the residuals for the subsequent cranks at 50% SOC and below remain below threshold. In contrast, at 50% SOC, the voltage based method generates ΔV values above threshold for cranks 1 and 3 and a ΔV value below threshold for crank 2.

Table 14: Field battery #69 at 25°C.

SOC		100% SOC		90% SOC		80% SOC		75% SOC	
		ΔV	r	ΔV	r	ΔV	r	ΔV	r
crank #	1	1.156	-1.136	1.294	**-1.518**	0.914	**-2.055**	**0.025**	**-2.532**
	2	1.073	**-1.231**	0.825	**-1.723**	0.779	**-2.351**	**-0.537**	**-3.110**
	3	1.357	**-1.283**	**0.628**	**-1.858**	**0.306**	**-2.414**	**failure**	**failure**

Table 14 reports the comparative results for battery #69. The battery failed to crank the vehicle at the 3rd crank of 75% SOC and at the next SOC level below 75%. At 100% SOC (above the *SOC_Threshold* of 60%), the residual values generated by the parity-relation based algorithm are below the threshold of -1.2. Thus, the algorithm would issue a pre-warning message of "Replace Battery". At 90% SOC (above the *SOC_Threshold* of 60%), the voltage based algorithm issues the same pre-warning message of "Replace Battery". Both

algorithms are capable of offering a timely pre-warning to avoid cranking failure at 75% SOC. However, the parity-relation based method offers an earlier pre-warning and is more consistent than the voltage based method. For instance, at 90% and 80% SOC, respectively, the parity-relation method is more consistent than the voltage based method because residuals below threshold are generated for all 3 cranks at each SOC level. In contrast, the voltage based method only generates ΔV values below threshold for crank 3 at 90% and 80% SOC, respectively. The messages offered by both algorithms are consistent with the message issued from the Midtronics battery tester of "Replace Battery".

5.3.2 Comparison of SOH Monitoring Methods Using JCI LN3 Batteries

This section describes the comparison of the ΔV and residual values generated from vehicle cranking data collected weekly throughout the accelerated aging process from 10 JCI LN3 production batteries at high SOC (approximately 100%) and 25°C. The batteries were aged using accelerated aging procedures from fresh to end-of-life. Weekly vehicle cranking was conducted at high SOC and 25°C for each battery. The SOH monitoring algorithms described in Section 3.3 and Section 4.4 were applied to determine the SOH of each battery.

Below, illustrative examples are presented that represent a comparison of the SOH monitoring algorithms using ΔV and residual values generated from vehicle cranking data collected weekly from 10 JCI LN3 batteries at a high SOC and 25°C. In the following tables, each week is denoted as a test period. The calibration values for $\underline{\Delta V\_Threshold}$ and $\underline{SOC\_Threshold}$ at 25°C are 0.7 volts and 60% SOC, respectively.

The calibration values for *r Threshold* and *SOC_Threshold* at 25°C are -1.2 volts and 60% SOC, respectively. Thus, in the following analysis, when ΔV falls below 0.7 volts or *r* falls below -1.2 volts, the algorithms issue a recommendation of "Replace Battery", since 100% SOC is above the 60% SOC threshold. For each table, the last test period presented is one test period (i.e., one week) prior to cranking failure.

Additionally, in the following tables, residual cells with the remark "bad data" indicate that the collected current data, $I(t)$, was corrupted. Thus, the residual values for those cranks cannot be calculated.

Table 15: Battery JCI005 (high SOC at 25°C).

crank #	Test Period 1		Test Period 2		Test Period 3		Test Period 4	
	ΔV	r	ΔV	r	ΔV	r	ΔV	r
1	1.303	0.135	1.037	0.045	0.988	0.027	0.971	-0.023
2	1.297	0.156	1.319	0.080	1.041	0.099	0.967	-0.009
3	1.085	0.174	1.044	0.077	1.106	0.104	0.945	0.002

crank #	Test Period 5		Test Period 6		Test Period 7		Test Period 8	
	ΔV	r	ΔV	r	ΔV	r	ΔV	r
1	1.213	0.005	1.123	-0.031	0.977	-0.048	1.224	-0.087
2	1.273	0.019	1.138	0.045	1.147	bad data	1.234	0.022
3	1.153	0.020	1.134	0.057	1.123	bad data	1.259	0.030

crank #	Test Period 9		Test Period 10	
	ΔV	r	ΔV	r
1	1.234	-0.371	**-1.666**	**-2.904**
2	1.020	-0.360	**0.384**	**-2.804**
3	1.098	-0.385	**0.260**	**-2.767**

Table 15 shows the comparative results for LN3 battery JCI005. The battery failed to crank the vehicle at test period 11. For test periods 1-9, both the ΔV and residual values are above the thresholds of 0.7 and -1.2, respectively. During test period 10, the ΔV and residual values fall below their respective thresholds. Thus, both of the algorithms

are capable of issuing the recommendation of "Replace Battery" at test period 10, hence avoiding cranking failure at test period 11.

Table 16: Battery JCI008 (high SOC at 25°C).

crank #	Test Period 1		Test Period 2		Test Period 3		Test Period 4	
	ΔV	r	ΔV	r	ΔV	r	ΔV	r
1	1.398	0.506	1.241	0.481	1.152	0.437	1.161	0.399
2	1.277	0.442	1.347	0.490	1.345	0.413	1.100	0.432
3	1.264	0.483	1.053	0.497	1.256	0.429	1.240	0.460

crank #	Test Period 5		Test Period 6		Test Period 7	
	ΔV	r	ΔV	r	ΔV	r
1	1.091	0.393	1.328	0.281	**-0.994**	**-3.411**
2	1.173	0.378	1.267	0.249	**-0.791**	**-3.429**
3	1.255	0.395	1.343	0.263	**-0.783**	**-3.396**

Table 16 shows the comparative results for LN3 battery JCI008. The battery failed to crank the vehicle at test period 8. Both algorithms issue the message of "Replace Battery" for all 3 cranks of test period 7 since ΔV and residual values are well below their respective thresholds. Hence, both algorithms provide a timely pre-warning before cranking failure at test period 8.

CHAPTER 6

SUPPORT VECTOR MACHINE BASED SOH MONITORING METHOD

This chapter describes a support vector machine (SVM) based pattern recognition method to monitor battery SOH utilizing the features of battery voltage and engine cranking speed. This method provides a percentage based prognosis of the SOH of a battery. In this research, a correlation between engine cranking speed and battery SOH has been observed. Engines cranked with aged batteries or batteries with low cranking power capability tend to have longer than normal cranking times (i.e., $\leq 1\,\text{second}$). Due to the difficulty in developing a good mathematical model that incorporates the various engine parameters involved in the engine cranking process, a qualitative or model-less approach is chosen. Rather than construct a physics-based model, a statistical model is trained with data characterizing fresh batteries and aged batteries. An obvious advantage of the SVM approach is that a highly sophisticated mathematical model is not required. Another advantage is the SVM ability to handle rather large data sets.

In this research, the SVM toolbox, LIBSVM, developed by Chang and Lin [38] was used. This SVM method was applied to the vehicle cranking data obtained from 10 JCI LN3 production batteries tested weekly at high SOC (nearly 100% SOC) and 25°C in order to determine battery SOH. Because the variation of engine condition in the test vehicle was reduced, the cranking time can be considered as a measure of the battery's

actual cranking SOH. Therefore, the battery voltage data during cranking and the corresponding engine cranking speed data from fresh and aged batteries were selected as training data for the SVM. Using this training data, the SVM constructs the optimal hyperplane in order to classify previously unseen test data. The SVM classifies unseen cranking data as either fresh or aged and generates a probability estimate of correct classification which is used to determine the SOH of the battery at each test crank. This SVM is capable of determining the SOH of the 10 JCI LN3 batteries based on the voltage and rpm data extracted from the batteries during cranking. Moreover, the effectiveness of the SVM method has been verified using the battery cranking voltage and parity-relation methods as references.

In Section 6.1, an overview of support vector machines is presented. Section 6.2 details the motivation and analysis of the proposed technical approach. Section 6.3 presents examples of the evaluation results obtained using the SVM approach and the 10 JCI LN3 batteries that were tested weekly at high SOC and 25°C.

6.1 Support Vector Machines

A support vector machine is a supervised learning algorithm based on statistical learning theory developed by Vladimir Vapnik and his team at AT&T Bell Labs in the 1990's. Support vector machines are capable of classification and regression [39]. They are used in real-world applications such as object detection, face or text recognition, and classification of gene expressions data. Support vector machines possess key advantages over traditional classifiers. SVM can potentially handle very large feature spaces. Unlike conventional classifiers, SVM is efficient in large classification problems because

the dimension of classified training vectors doesn't significantly influence the performance of the SVM [40]. Also, SVM has better generalization performance compared to conventional classifiers. SVM aims to minimize the structural risk by minimizing an upper bound of the generalization error whereas conventional methods seek to minimize the empirical risk by minimizing training error [41].

The objective of the support vector machine is to construct a decision boundary from classified training data in order to classify future test data. The SVM determines an optimal decision boundary (hyperplane) that separates the classes to which the training data belong and maximizes the separation between the training data from each class. The SVM minimizes its risk of misclassifying previously unseen data by selecting the hyperplane that maximizes the margin between the sets of training data [39].

Training data is input as vectors in n-dimensions and assigned a classification label (e.g., -1 or 1). If the data is linearly inseparable, it can be mapped into a higher dimension feature space using a kernel function. The kernel function is a mathematical function that projects data from a low-dimensional space to a higher-dimensional space [39]. If chosen correctly, the kernel function produces data that is linearly separable in the higher dimensional space.

Once the data is projected into this higher-dimensional feature space, the SVM determines a decision boundary or separating hyperplane in order to maximize the margin between the separating hyperplane and the data sets. The maximum margin is determined by constructing two parallel hyperplanes, one on each side of the separating hyperplane, that provide maximum separation between the feature vectors from each data set. In order to maximize the margin between the data sets, the two parallel hyperplanes

are selected such that the maximum distance between the hyperplanes is achieved with the minimum number of feature vectors inside the margin. Vectors lying on the two determined hyperplanes are called support vectors. The separating hyperplane is then projected back down onto the lower-dimensional input space.

The remainder of Section 6.1 discusses important features central to the performance of support vector machines and the SVM specific to this research. In Section 6.1.1, the determination of the maximum-margin hyperplane is discussed in detail. The kernel function is described in Section 6.1.2, and Section 6.1.3 covers the classification of test data and probability estimates generated from SVM.

6.1.1 Determining the Maximum-Margin Hyperplane

This section describes how the optimal hyperplane is constructed for a two-class linearly separable data set. Let the feature vectors of the training set, *X*, be the n-dimensional input x_i, (i = 1, 2, …, N, N is the number of samples) with associated labels $y_i = 1$ for class ω_1 or $y_i = -1$ for class ω_2 [42][43]. The goal is for the SVM to determine a hyperplane (i.e., a line in this case), to correctly classify all of the training vectors, of the form given in (31), where w is the direction of the hyperplane and b is its position in space.

$$\begin{aligned} g(x) &= sign(f(x)), \\ f(x) &= w^T x + b = 0 \end{aligned} \tag{31}$$

There are many such hyperplanes that satisfy (31). For example, Figure 25 illustrates a linear separable two class training data set with two separating hyperplanes selected from an infinite number of possible separating hyperplanes. The data points in the upper portion of the plot, marked as dots, are of class ω_1, and the data points in the lower portion of the plot, marked as x, are of class ω_2. Although each hyperplane correctly classifies the training data, the optimal hyperplane will minimize the risk of misclassification of unseen future data. The hyperplane which maximizes the margin on either side of it from the nearest data points from each class is optimal for minimizing the risk of misclassification.

The SVM aims to find the location and direction of the hyperplane which not only correctly classifies all the training data but also gives the maximum possible margin between the two classes [42]. The distance of a point from a hyperplane is given by (32), where $|f(x)|$ is the Euclidean distance of a point from the hyperplane.

$$z = \frac{|f(x)|}{\|w\|}, \tag{32}$$

$$\|w\| = \sqrt{w_1^2 + w_2^2}\ . \tag{33}$$

The distances from the nearest points in each class to their respective hyperplanes are denoted z_1 and z_2. It can be seen that hyperplane (H_2) with margin $2z_2$ has a larger

margin than hyperplane (H_1). Thus, the increased margin of hyperplane (H_2) has a lower associated risk of misclassification compared to hyperplane (H_1).

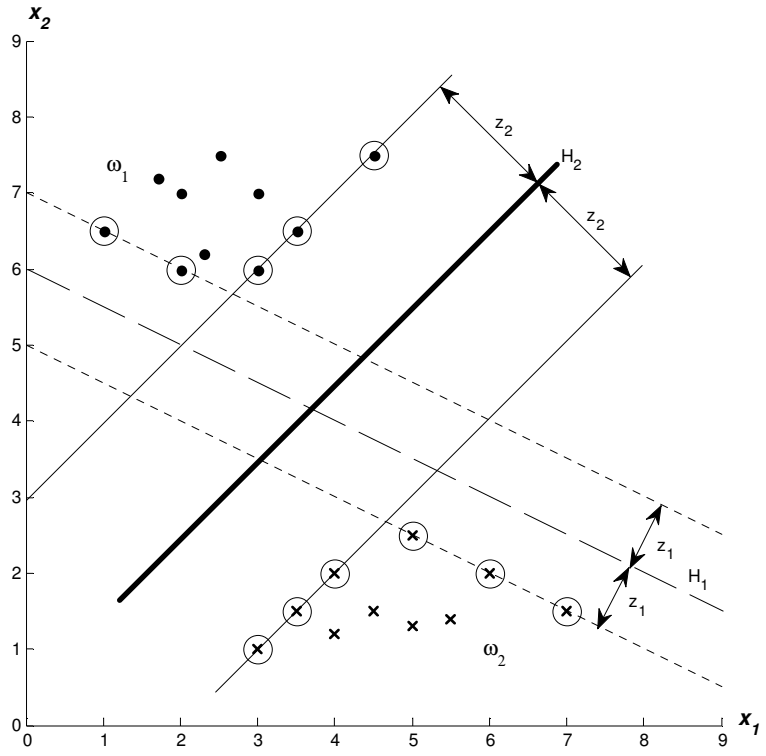

Figure 25: Two possible locations and directions of separating hyperplanes.

By scaling w and w_0, the value of $f(x)$ at the points closest to the hyperplanes in ω_1 and ω_2 (circled in Figure 25) become equal to (+1) for class ω_1 and (-1) for class ω_2. Thus, the hyperplane will have a margin given in (34) such that the linear inequality constraints given in (35) are satisfied.

$$\frac{1}{\|w\|} + \frac{1}{\|w\|} = \frac{2}{\|w\|} \tag{34}$$

$$\begin{aligned} w^T x + b &\geq 1, \quad \forall x \in \omega_1 \\ w^T x + b &\leq -1, \quad \forall x \in \omega_2 \end{aligned} \tag{35}$$

Minimizing the norm will afford the maximum margin. The separating hyperplane that maximizes the distance between itself and the nearest data from each class is the optimal separating hyperplane. The parameters *w* and *b* of the maximum-margin hyperplane can be found by solving the following convex quadratic optimization problem subject to a set of linear inequality constraints.

$$\text{minimize} \quad J(w) \equiv \frac{1}{2}\|w\|^2 \tag{36}$$

$$\text{subject to} \quad y_i(w^T x_i + b) \geq 1, \ i = 1,2,...,N \tag{37}$$

The minimizer must satisfy the following Karush-Kuhn-Tucker (KKT) conditions [42], where λ is the vector of Lagrange multipliers, λ_i.

$$\frac{\partial}{\partial w} L(w,b,\lambda) = 0 \tag{38}$$

$$\frac{\partial}{\partial b} L(w,b,\lambda) = 0 \tag{39}$$

$$\lambda_i \geq 0, \quad \forall i \tag{40}$$

$$\lambda_i[y_i(w^T x_i + b) - 1] = 0, \quad \forall i \tag{41}$$

The Lagrangian function, $L(w,b,\lambda)$, is defined in (42) as

$$L(w,b,\lambda) = \frac{1}{2} w^T w - \sum_{i=1}^{N} \lambda_i [y_i (w^T x_i + b) - 1] \tag{42}$$

Combining (42) with (38) and (39) results in

$$w = \sum_{i=1}^{N} \lambda_i y_i x_i \tag{43}$$

$$\sum_{i=1}^{N} \lambda_i y_i = 0 \tag{44}$$

Since $\lambda_i \geq 0$, the vector *w* of the maximum-margin hyperplane is a linear combination of the feature vectors with active constraints $\lambda_i \neq 0$. Hence, the support vectors lie on either of the two hyperplanes parallel to the separating hyperplane with equations (45).

$$w^T x + b = \pm 1 \tag{45}$$

The support vectors are the training vectors that are closest to the decision boundary (separating hyperplane). The parameter *b* can be obtained from any of the conditions in (41) satisfying $\lambda_i \neq 0$.

To simplify the calculations, the problem with KKT conditions can be converted into the equivalent Wolfe dual representation form [42][44].

$$\text{maximize} \quad L(w, b, \lambda) \tag{46}$$

$$\text{constrained by} \quad w = \sum_{i=1}^{N} \lambda_i y_i x_i \tag{47}$$

$$\sum_{i=1}^{N} \lambda_i y_i = 0 \tag{48}$$

$$\lambda \geq 0 \tag{49}$$

Substituting (47) and (48) into (46), the equivalent optimization task is to

$$\text{maximize} \quad W(\lambda) = \sum_{i=1}^{N} \lambda_i - \frac{1}{2} \sum_{i,j=0}^{N} \lambda_i \lambda_j y_i y_j x_i^T x_j \tag{50}$$

$$\text{subject to} \quad \sum_{i=1}^{N} \lambda_i y_i = 0 \tag{51}$$

$$\lambda \geq 0 \tag{52}$$

After calculating the Lagrange multipliers via (50), the parameter *w* of the maximum-margin hyperplane is obtained from (47) and *b* from (41) as before.

Figure 26 illustrates the graphical results of solving the convex quadratic optimization problem to determine the maximum-margin hyperplane. The support vectors (circled) constitute the critical elements from the set of training vectors. They lie closest to the decision boundary (separating hyperplane) on the two parallel hyperplanes, h_1 and h_2, described by $w^T x + b = \pm 1$, respectively. These support vectors will have Lagrange multipliers $\lambda_i \geq 0$. All other training vectors not on h_1 and h_2 will have values

of $\lambda_i = 0$. Note that $\frac{|b|}{\|w\|}$ is the perpendicular distance from the separating hyperplane (i.e., the dark solid line) to the origin along the vector *w* [44].

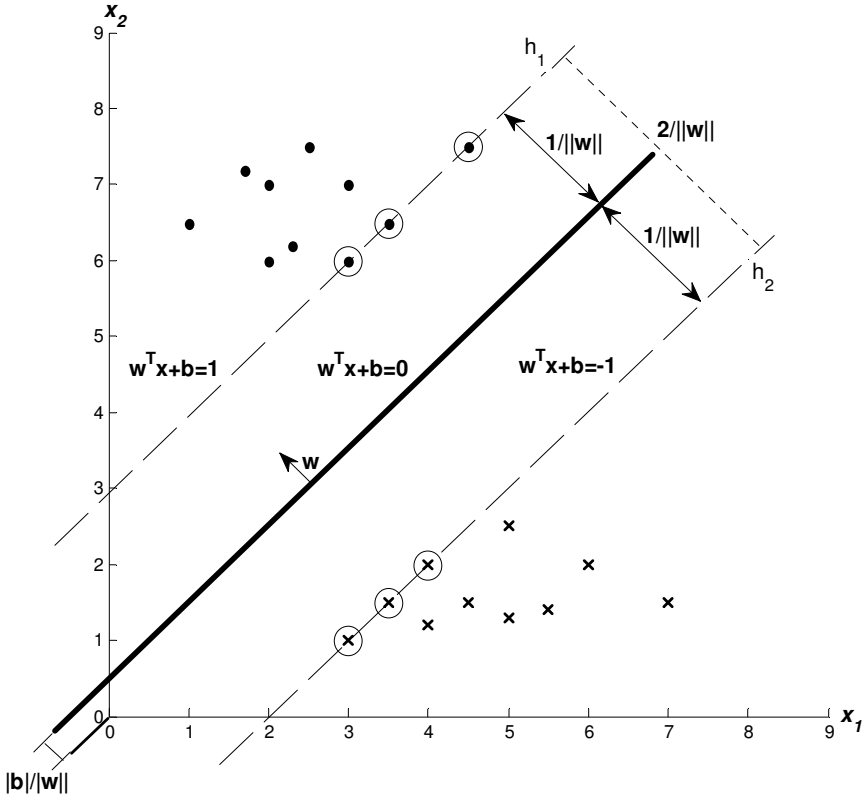

Figure 26: The maximum-margin hyperplane for a two class linearly separable data set.

6.1.2 The Kernel Function

The kernel function is a function that projects the training data from a low-dimensional space into a higher-dimensional space with the aim of creating a linearly separable data set in the higher-dimensional space. It allows SVM to separate data with complex boundaries. From [45], a kernel is defined as a function *K*, such that for all $x, z \in X$,

$$K(x, z) = \langle \phi(x) \cdot \phi(z) \rangle \tag{53}$$

where ϕ maps the images of the two arguments (x, z) from X to a dot product feature space. Some common kernel functions used are

- Linear: $K(x, z) = \langle x, z \rangle$ (54)
- Polynomial: $K(x, z) = (x^T z + 1)^q, \quad q > 0$ (55)
- Radial Basis Function: $K(x, z) = \exp\left(-\frac{\|x - z\|^2}{\sigma^2} \right)$ (56)
- Hyperbolic Tangent: $K(x, z) = \tanh(\beta x^T z + \gamma)$ (57)

The kernel function may cause over-fitting where numerous boundaries are constructed that are specific to certain data from the training data [39]. Projecting into a high-dimensional space can create difficulty for the algorithm to select the correct solution because the number of possible solutions increases exponentially as the number of variables increase.

6.1.3 Classifying Test Data and Probability Estimates

Once the SVM has been trained, it is used to classify previously unseen test data. For a two class classifier, the SVM from LIBSVM [38], assigns class labels according to a "Max Wins" voting strategy. For each test data point x_i, the decision boundary (separating hyperplane) function $g(x_i) = \text{sign}(w^T x_i + b)$ is evaluated. If $g(x_i) > 0$, then x_i is in the class corresponding to $y = 1$. The vote for this class is added by one.

Otherwise, the vote is increased by one for the class corresponding to $y = -1$. Then, x is predicted to be in the class with the most votes. In the case of a tie in the voting method, x is labeled with the class having the smallest index [46].

Obviously, correct classification is of great importance in this SVM method to determine battery SOH. Equally important are the posterior probabilities for each class, that this SVM is capable of offering. The posterior probability is the probability that x belongs to a certain class. More formally, given k data classes, the LIBSVM package aims to estimate the posterior probability, for any x given by (58).

$$p_i = (y = i \mid x), \quad i = 1,...,k \,. \tag{58}$$

The posterior probabilities are estimated in LIBSVM by fitting a sigmoid function that maps the outputs g to posterior probabilities [46]. The following procedure outlines the estimation of posterior probabilities:

1) Estimate the pairwise class probabilities.

$$r_{i,j} = p(y = i \mid y = i \text{ or } j, x) \approx \frac{1}{1 + \exp(Ag + B)} \tag{59}$$

A and B are two parameters estimated by minimizing the negative log-likelihood function with known training data and their corresponding decision values. To obtain decision values, five-fold-cross-validation is conducted because class labels and decision values are required to be independent.

2) Obtain the p_i's by solving the optimization problem

$$\begin{aligned} \text{minimize } p \quad & \frac{1}{2}\sum_{i=1}^{k}\sum_{j:j\neq i}(r_{ji}p_i - r_{ij}p_j)^2 \\ \text{subject to} \quad & \sum_{i=1}^{k} p_i = 1 \\ & p_i \geq 0, \quad \forall i \end{aligned} \tag{60}$$

The SVM of LIBSVM returns the estimated posterior probabilities for both classes to which a test data point might belong. In Section 6.2, the use of these probabilities in determining the SOH of a battery will be discussed in further detail.

6.2 Analysis of Battery Cranking Voltage and Engine RPM Characteristics

Figure 27 shows the battery cranking voltage and engine cranking speed waveforms for one of the 10 JCI LN3 batteries tested weekly at high SOC (nearly 100% SOC) and 25°C.

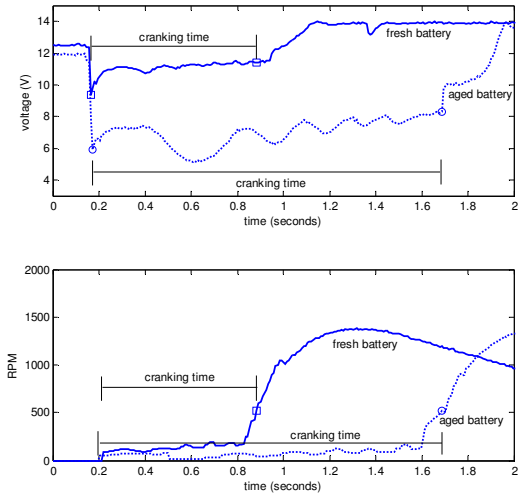

Figure 27: Battery cranking voltage and engine cranking speed waveforms of a fresh and aged battery.

The solid line voltage and rpm waveforms were collected during cranking at the beginning of the ageing procedure when the battery was fresh. The dashed line voltage and rpm waveforms are from the same battery at the end of the ageing procedure. The engine cranking time begins at the initial voltage drop when the starter motor is initially engaged (see Section 1.2). A successful engine crank corresponds to an engine cranking speed of approximately 500 rpm. As can be seen in the figure, for the aged battery, the cranking time is significantly longer than the cranking time of the fresh battery. Moreover, the aged battery requires greater voltage throughout the cranking process compared to the fresh battery due to greater voltage loss and/or increased battery resistance (see Section 3.2). It is this consistent observation with the 10 JCI LN3 batteries throughout the accelerated ageing cycling process that motivated the selection of the voltage and engine rpm data as training features for the SVM method to determine battery SOH.

The 10 JCI LN3 batteries were used to crank the engine of testing vehicle. The engine was kept running for approximately thirty-five minutes to warm up the engine oil temperature to approximately 90°C before conducting the cranking test. Therefore, the variation of the engine condition was reduced and the cranking time can be considered as a measure of the battery's actual cranking SOH. In real-world applications, cranking time is also sensitive to the health of other components of the starting system, for instance, the starter, engine oil condition, and the engine; therefore it cannot be directly used as a battery SOH indicator.

6.2.1 Training the Two-Class Support Vector Machine Classifier

To train the SVM, battery voltage and engine cranking speed signals representing fresh and aged batteries sampled every 50ms were selected and pre-processed to extract the voltage and engine rpm data corresponding to the short period of engine cranking (see, for example, Figure 27). Each voltage and corresponding engine rpm data point represents a training feature vector. Based on the maximum and minimum fresh battery voltages and corresponding maximum and minimum engine cranking speeds during cranking, the feature vectors are normalized from -1 to 1 and then assigned a class label (i.e., 1 for fresh and -1 for aged).

The SVM applies the radial basis kernel function (see Section 6.1.2), to project the scaled feature vectors into a higher-dimensional feature space and construct the maximum-margin hyperplane (see Section 6.1.1). Figure 28 shows the scaled training feature vectors from aged and fresh batteries used to construct the SVM training model to

determine battery SOH. As can be seen in the figure, the training feature vectors are linearly separable, thus, this SVM is a two-class linear classifier.

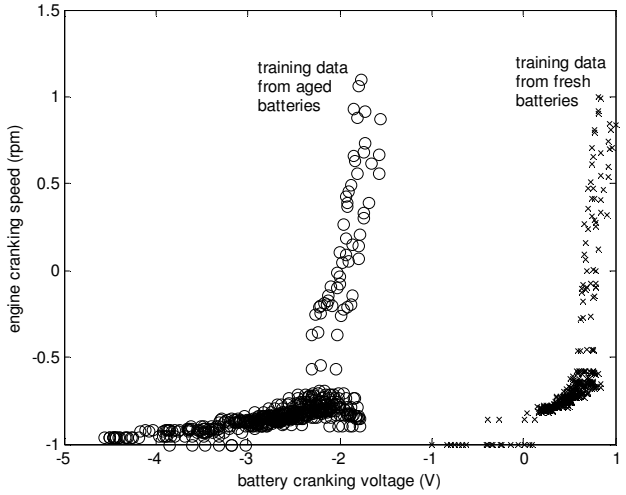

Figure 28: Scaled voltage and rpm training data from aged and fresh batteries during cranking.

6.2.2 Testing the SVM Two-Class Classifier

Once the SVM model has been trained, it is used to classify previously unseen battery voltage and engine cranking speed data to verify its performance and determine the SOH of the 10 JCI LN3 batteries. The SVM classifies test data and provides estimated posterior probabilities. The estimated probabilities are used to predict the SOH of the battery at each week.

The inputs to the SVM are the battery voltage and engine cranking speed at a sampling rate of 50ms. The specifications of the sensor signals and variables are listed in Table 17.

Table 17: Specifications of sensor signals and variables.

Battery signals	accuracy	resolution	range	sampling rate
Voltage (V)	± 0.1	0.001	0 to 16	50 ms
Engine Cranking Speed (RPM)	±0.1	0.1	0 to 2000	50 ms

As in SVM training, the voltage and rpm data input during testing is pre-processed to extract the battery voltage and engine rpm data corresponding to the short period of cranking (see, for example, Figure 27). The voltage and rpm feature vectors are also scaled from -1 to 1 based on the maximum and minimum fresh battery voltage during training and corresponding maximum and minimum engine cranking speeds, respectively. The SVM classifies each sampled data vector using the voting method and returns the estimated posterior probabilities of each of the N test vectors belonging to the fresh battery and the aged battery classes (see Section 6.1.3). The posterior probabilities for each test vector belonging to the fresh battery class (1 for fresh batteries) are averaged and multiplied by 100% to obtain the predicted SOH percentage of the battery for a given week. The remaining SOH of the battery as a percentage for one crank at each week is given by (61) and (62).

$$p_i(y=1 \mid x) = \begin{bmatrix} p_1 \\ p_2 \\ \vdots \\ p_N \end{bmatrix}, \text{ where } N = \text{total number of test vectors} \tag{61}$$

$$\text{battery SOH } (\%) = \frac{\sum_{i=1}^{N} p_i}{N} * 100\% \tag{62}$$

6.3 SVM Performance Evaluation Using LN3 Battery Cranking Data

In this section, a few examples of the SVM performance evaluation results are presented. The vehicle cranking data was collected weekly throughout an accelerated aging process from JCI LN3 batteries at high SOC (approximately 100%) and 25°C. Through analysis of the SVM evaluation results for the 10 JCI LN3 batteries, to provide a timely pre-warning of cranking failure, a *SOH_Threshold* of 40% is calibrated. Thus, in the following analysis, when the SOH percentage falls below 40%, a recommendation of "Replace Battery" would be issued to prevent subsequent cranking failure.

The results of the SVM state-of-health estimate are compared to a cranking time based SOH. The cranking time based SOH is used as a reference to verify the effectiveness of the SVM method. Again, because the variation of engine condition in the test vehicle was kept minimal, cranking time may be used as a measure of the battery's actual cranking SOH. The cranking time based SOH algorithm generates an SOH percentage for each crank at each week by comparing the current cranking time to a calibrated nominal cranking time and cranking time threshold. The SOH percentage for each crank is given by (63), where t_{crank} is the current cranking time considered, t_{nom} is the nominal cranking time for fresh batteries, and t_{thresh} is the cranking time threshold between fresh and aged batteries.

$$\mathrm{SOH}(\%) = \frac{t_{crank} - t_{thresh}}{t_{nom} - t_{thresh}} * 100\%, \tag{63}$$

Each plot contains the cranking time based SOH and the SVM estimate of SOH as percentages ranging from 0% to 100%. Each test period is one week and the last test period is one week prior to cranking failure.

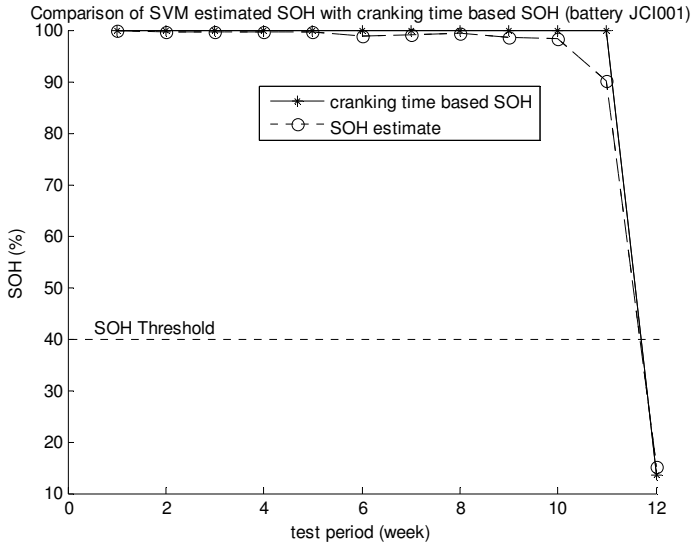

Figure 29: Battery JCI001 (high SOC at 25°C).

Figure 29 illustrates the results for LN3 battery JCI001. In the figure, the dashed line with markers (o) represents the SVM estimated battery SOH. The solid line with markers (*) represents the battery SOH determined by cranking time. The *SOH_Threshold* (dashed line) is illustrated at 40% SOH. The battery failed to crank the vehicle at test period 13. The SVM accurately predicts the SOH of the battery with respect to the cranking time based SOH. At test period 12, the cranking time based SOH of battery JCI001 falls well below the *SOH_Threshold* of 40%. The SVM method is capable of predicting the SOH of the battery at test period 12 and offers the pre-warning to "Replace Battery" to avoid pending cranking failure at test period 13.

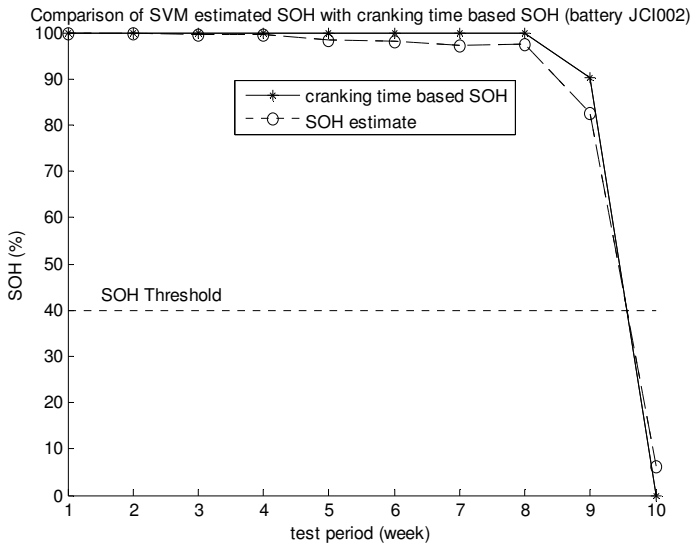

Figure 30: Battery JCI002 (high SOC at 25°C).

Figure 30 illustrates the results for LN3 battery JCI002. The battery failed to crank the vehicle at test period 11. For test periods 1-10, the SVM closely predicts the SOH of the battery with respect to the cranking time based SOH. At test period 10, the SVM estimates the battery SOH to be well below the *SOH_Threshold* of 40%. Hence, the SVM is capable of offering the pre-warning of "Replace Battery" at test period 10 to avoid pending cranking failure at the following week.

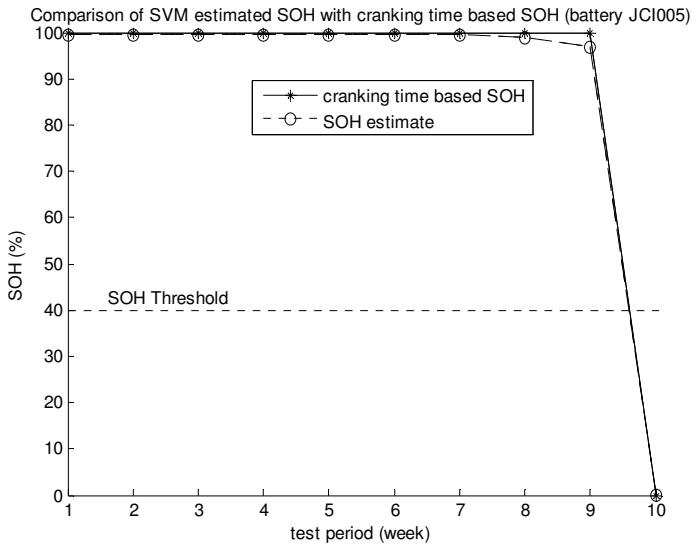

Figure 31: Battery JCI005 (high SOC at 25°C).

Figure 31 illustrates the results for LN3 battery JCI005. The battery failed to crank the vehicle at test period 11. For all test periods, the SVM closely approximates the battery SOH with respect to the cranking time based battery SOH. For test period 10, the SVM predicts the battery SOH at or near 0%. Therefore, the SVM accurately estimates the battery SOH with respect to the cranking time based SOH throughout the ageing process and is capable of offering the pre-warning of "Replace Battery" to avoid pending cranking failure at test period 11.

CHAPTER 7

CONCLUSION AND FUTURE RESEARCH WORK

Four battery SOH monitoring methods, including a battery cranking voltage based approach, a parity-relation based approach, a conventional resistance based approach, and a support vector machine based pattern recognition approach, have been researched and presented within this thesis. The battery cranking voltage based method and the parity-relation based method are capable of providing pre-warnings of pending vehicle cranking failure due to low battery SOH. Both of these methods are more robust than the conventional resistance based method with respect to battery type variations. A key advantage of the cranking voltage based method is that a costly high current sensor is not required. Moreover, compared with conventional SOH monitoring methods based on model parameters of an equivalent circuit battery model, calibration of the algorithm is easier.

With the addition of a high current sensor, the parity-relation based method is more consistent than the cranking voltage based method. The parity-relation based method combines the SOH information provided by both battery resistance and battery voltage loss during cranking, hence achieving better diagnostic/prognostic performance.

Finally, the support vector machine based pattern recognition approach utilizes features of battery voltage and engine cranking speed during engine cranking. This

method can also offer a pre-warning of pending cranking failure and does not require a costly high current sensor. The SVM was evaluated on engine cranking data collected in a very controlled environment. The results are preliminary and will require further development and testing with batteries at various conditions to verify consistent and robust performance as a battery SOH monitoring method.

The battery cranking voltage and parity-relation based algorithms discussed within this thesis are capable of offering recommendations prior to battery end-of-life based on battery cranking power capability. However, neither method offers any indication of the actual battery capacity remaining. Future work includes developing more sophisticated battery monitoring methods that provide accurate SOC control and are capable of determining battery SOH based on battery capacity.

The SVM pattern recognition method is capable of predicting battery SOH and offering a pre-warning of pending cranking failure. Moreover, the SVM method generates a percentage-based prognosis of battery cranking power capability. Developing methods that provide a prognosis of the remaining useful life of a battery in terms of mileage is a more attractive feature that will be explored in future research work.

REFERENCES

[1] A. Emadi, M. Ehsani, and J. M. Miller, *Vehicular Electric Power Systems*, New York: Marcel Dekker, 2004.

[2] M. Koot, J. T. B. A. Kessels, B. de Jager, W. P. M. H. Heemels, P. P. J. van den Bosch, and M. Steinbuch, "Energy management strategies for vehiclular electric power systems," *IEEE Transactions on Vehicular Technology*, vol. 54, no. 3, May 2005.

[3] P. Popp, M. Salman, Y. Zhang, X. Zhang, and Y.-K Chin, "Vehicle Diagnosis and Prognosis: Concepts, Trends, and Applications to Batteries," *Proceedings of Convergence*, 2006.

[4] E. Meissner and G. Richter, "The change to the automotive battery industry: the battery has to become an increasingly integrated component within the vehicle electric power system," *Journal of Power Sources*, vol. 156, pp. 438-460, 2005.

[5] M. Schollmann, M. Rosenmayr, and J. Olk, "Battery monitoring with the intelligent battery sensor during service, standby and production," SAE 2005-01-0561.

[6] M. Cox and K. Bertness, "Vehicle-integrated battery and power system management based on conductance technology to enable intelligent generating systems (inGEN)," SAE 01TB-128.

[7] H. Blanke, O. Bohlen, S. Buller, et al., "Impedance measurements on lead-acid batteries for state-of-charge, state-of-health and cranking capability prognosis in electric and hybrid electric vehicles," *Journal of Power Sources*, no. 144, pp. 418-425, 2005.

[8] E. Meissner, G. Richter, "Vehicle electric power systems are under change! Implications for design, monitoring, and management of automotive batteries," *Journal of Power Sources*, no. 95, pp. 12-23, 2001.

[9] F. Huet, "A review of impedance measurements for determination of state-of-charge or state-of-health of secondary batteries," *Journal of Power Sources*, vol. 70, pp. 59-69, 1998.

[10] E. Chowanietz, *Automobile Electronics*. London: Reed Elsevier, 1995.

[11] D. Berndt, *Maintenance-Free Batteries.* Baldock, Hertfordshire, England: Research Studies Press LTD., 2003.

[12] E. Meissner and G. Richter, "Battery monitoring and electrical energy management precondition for future vehicle electric power systems, *Journal of Power Sources*, vol. 116, pp. 79-98, 2003.

[13] M. Coleman, C.B. Zhu, C.K. Lee, and W.G. Hurley, "A combined SOC estimation method under varied ambient temperature for a lead-acid battery," *Applied Power Electronics Conference and Exposition*, vol. 2, pp. 991-997, March 2005.

[14] T. Hansen and C.-J. Wang, "Support vector based battery state of charge estimator," *Journal of Power Sources*, vol. 141, pp. 351-358, 2005.

[15] P. Ruetschi, "Aging mechanisms and service life of lead-acid batteries," *Journal of Power Sources*, vol. 127, pp. 33-44, 2004.

[16] R. Isermann, "Process fault detection based on modeling and estimation methods: a survey," *Automatica*, vol. 20, pp. 387-404, 1984.

[17] R. Isermann, "Supervision, fault-detection and fault-diagnosis methods – an introduction," *IFAC Control Engineering Practice*, vol. 5, pp. 639-652, 1997.

[18] P.M. Frank, "Analytical and qualitative model-based fault diagnosis – a survey and some new results," *European Journal of Control*, vol. 2, pp. 6-28, 1996.

[19] S. Leonhardt and M. Ayoubi, "Methods of fault diagnosis," *Control Engineering Practice*, vol. 5, pp. 683-692, 1997.

[20] J. Lunze, "Qualitative modeling of linear dynamical systems with quantized state measurements," *Automatica*, vol. 30, pp. 417-431, 1994.

[21] B. Hariprakash, S.K. Martha, A. Jaikumar, and A.K. Shukla, "On-line monitoring of lead-acid batteries by galvanostatic non-destructive technique," *Journal of Power Sources*, vol. 137, pp. 128-133, 2004.

[22] A. Salkind, C. Fennie, P. Singh, T. Atwater, and D.E. Reisner, "Determination of state-of-charge and state-of-health of batteries by fuzzy logic methodology," *Journal of Power Sources*, vol. 80, pp. 293-300, 1999.

[23] B.S. Bhangu, P. Bentley, D.A. Stone, and C.M. Bingham, "Nonlinear observers for predicting state-of-charge and state-of-health of lead-acid batteries for hybrid-electric vehicles," *IEEE Transactions on Vehicular Technology*, vol. 54, no. 3, May 2005.

[24] X. Zhang, R. Grube, K. Shin, and M. Salman, "Automotive battery state-of-health monitoring: a battery cranking voltage based approach," *Integrated Systems Health Management Conference*, Covington, Kentucky, August 2008.

[25] X. Zhang, R. Grube, K. Shin, and M. Salman, "Automotive battery state-of-health monitoring: a parity-relation based approach," submitted to *The 7th IFAC Symposium on Fault Detection, Supervision, and Safety of Technical Processes*, Barcelona, Spain, 2009.

[26] A. Jossen, "Fundamentals of battery dynamics," *Journal of Power Sources*, vol. 154, pp. 530-538, March 2006.

[27] M. Verbrugge, D. Frisch, and B. Koch, "Adaptive energy management of electric and hybrid electric vehicles," *Journal of the Electrochemical Society*, vol. 152 (2), pp. A333-A342, 2005.

[28] S. Buller, M. Thele, E. Karden, R. W. De Doncker, "Impedance-based non-linear dynamic battery modeling for automotive applications," *Journal of Power Sources*, vol. 113, pp. 422-430, 2003.

[29] S.R. Nelatury and P. Singh, "Extracting equivalent circuit parameters of lead-acid cells from sparse impedance measurements," *Journal of Power Sources*, vol. 112, pp. 621-625, 2002.

[30] S. Rodrigues, N. Munichandraiah, and A.K. Shkla, "A review of state-of-charge indication of batteries by means of a.c. impedance measurements," *Journal of Power Sources*, vol. 87, pp. 12-20, 2000.

[31] X. Zhang, R. Grube, K. Shin, and M. Salman, "Automotive battery state-of-health monitoring: a battery cranking voltage based approach," *GM R&D Report*, CL-08-13-ECI, 2008a.

[32] J. J. Gertler, *Fault Detection and Diagnosis in Engineering Systems*, New York: Marcel Dekker, 1998.

[33] J. Chen and R. J. Patton, *Robust Model-Based Fault Diagnosis for Dynamic Systems*. Boston, MA: Kluwer, 1999.

[34] P. M. Frank, "Fault diagnosis in dynamic systems using analytical and knowledge-based redundancy – a survey and some new results," *Automatica*, vol. 26, pp. 459-474, 1990.

[35] X. Zhang and R. Conell, "A parity-relation based approach to starting, lighting, and ignition battery state-of-health monitoring: algorithm development," *GM R&D Report*, ECI-286/CES-290, 2007.

[36] X. Zhang, R. Grube, K. Shin, M. Salman, and R. Conell, "Automotive battery state-of-health monitoring: a parity-relation based approach," *GM R&D Report*, 2008b.

[37] X. Zhang, R. Grube, K. Shin, and M. Salman, "Automotive battery state-of-health monitoring: comparative studies," *GM R&D Report*, 2008c.

[38] C.-C. Chang and C.-J. Lin, LIBSVM: a library for support vector machines, 2001. Software available at http://www.csie.ntu.edu.tw/~cjlin/libsvm.

[39] W.S. Noble, "What is a support vector machine?," in *Nature Biotechnology*. Nature Publishing Group, vol. 24, no. 12. pp. 1565-1567, 2006.

[40] P. Kostka and E. Tkacz, "Support vector machine classifier with feature extraction stage as an efficient tool for atrial fibrillation detection improvement," in *Computer Recognition Systems* 2. M. Kurzynski et al., Eds., Berlin, Heidelberg: Springer-Verlag, 2007, ASC 45, pp. 356-363.

[41] H.W. Liu, "Predicting non-protein-coding RNA genes in Escherichia coli using SVM with signature descriptor," *The Second International Symposium on Optimization and Systems Biology*, Lijiang, China, 2008, pp. 287-293.

[42] S. Theodoridis and K. Koutroumbas, *Pattern Recognition*. San Diego: Academic Press, 2006.

[43] S. Pöyhönen, A. Arkkio, P. Jover, and H. Hyötyniemi, "Coupling pairwise support vector machines for fault classification," *Control Engineering Practice*, vol. 13, pp. 759-769, 2005.

[44] C.J.C. Burges, "A tutorial on support vector machines for pattern recognition," in *Data Mining and Knowledge Discovery*. Boston: Kluwer Academic Publishers, 1998, pp. 121-167.

[45] N. Cristianini and J. Shawe-Taylor, *An Introduction to Support Vector Machines*. Cambridge University Press, 2000.

[46] C.-W. Hsu and C.-J. Lin, "A comparison of methods for multiclass support vector machines," *IEEE Transactions on Neural Networks*, vol. 13, no. 2, pp. 415-425, March 2002.

[47] M. Salman, N.S. Kapsokavathis, X. Zhang, D.W. Waters, X. Tang, "Method and apparatus for monitoring an electrical energy storage device," GM Patent filed, US Provisional Serial No: 60/871458, 2006.

[48] S. Gudmundsson, T.P. Runarsson, and S. Sigurdsson, "Automatic sleep staging using support vector machines with posterior probability estimates," *Proceedings of the 2005 International Conference on Computational Intelligence for Modelling, Control and Automation*, 2005.

[49] C.-C. Chang and C.-J. Lin, "LIBSVM: a library for support vector machines," Department of Computer Science, National Taiwan University, 2008. URL http://www.csie.ntu.edu.tw/~cjlin/papers/libsvm.pdf.

[50] R. Bi, Y. Zhou, F. Lu, and W. Wang, "Predicting gene ontology functions based on support vector machines and statistical significance estimation," *Neurocomputing*, vol. 70, pp. 718-725, 2007.

[51] D. Berndt, "Valve-regulated lead-acid batteries," *Journal of Power Sources*, vol. 100, pp. 29-46, 2001.

[52] E. Osuna, R. Freund, and F. Girosi, "Training support vector machines: an application to face detection," *Center for Biological and Computational Learning and Operations Research Center*, M.I.T., Cambridge, MA, pp. 130-136, 1997.